TISSUE ENGINEERING: Part A
Volume 19, Numbers 17 and 18, 2013

DOI: 10.1089/ten.tea.2012.0425.rev

Depolarization Alters Phenotype, Maintains Plasticity of Predifferentiated Mesenchymal Stem Cells

Sarah Sundelacruz, PhD,[1] Michael Levin, PhD,[2] and David L. Kaplan, PhD[1]

Although adult stem cell transplantation has been implemented as a therapy for tissue repair, it is limited by the availability of functional adult stem cells. A potential approach to generate stem and progenitor cells may be to modulate the differentiated status of somatic cells. Therefore, there is a need for a better understanding of how the differentiated phenotype of mature cells is regulated. We hypothesize that bioelectric signaling plays an important role in the maintenance of the differentiated state, as it is a functional regulator of the differentiation process in various cells and tissues. In this study, we asked whether the mature phenotype of osteoblasts and adipocytes derived from human mesenchymal stem cells (hMSCs) could be altered by modulation of their membrane potential. hMSC-derived osteoblasts and adipocytes were depolarized by treatment with ouabain, a Na^+/K^+ ATPase inhibitor, or by treatment with high concentrations of extracellular K^+. To characterize the effect of voltage modulation on the differentiated state, the depolarized cells were evaluated for (1) the loss of differentiation markers; (2) the up-regulation of stemness markers and stem properties; and (3) differences in gene expression profiles in response to voltage modulation. hMSC-derived osteoblasts and adipocytes exhibited significant down-regulation of bone and fat tissue markers in response to depolarization, despite the presence of differentiation-inducing soluble factors, suggesting that bioelectric signaling overrides biochemical signaling in the maintenance of cell state. Suppression of the osteoblast or adipocyte phenotype was not accompanied by up-regulation of genes associated with the stem state. Thus, depolarization does not activate the stem cell genetic signature and, therefore, does not induce a full reprogramming event. However, after transdifferentiating the depolarized cells to evaluate for multi-lineage potential, depolarized osteoblasts demonstrated improved ability to achieve correct adipocyte morphology compared with nondepolarized osteoblasts. The present study thus demonstrates that depolarization reduces the differentiated phenotype of hMSC-derived cells and improves their transdifferentiation capacity, but does not restore a stem-like genetic profile. Through global transcript profiling of depolarized osteoblasts, we identified pathways that may mediate the effects of voltage signaling on cell state, which will require a detailed mechanistic inquiry in future studies.

Introduction

Human mesenchymal stem cells (hMSCs) are a promising cell source for adult stem cell transplantation therapy for a range of tissues, including bone, cartilage, vasculature, skin, cardiovascular, and renal tissues.[1–4] While some success has been reported utilizing these cells for tissue repair, their clinical efficacy is hampered by the limited supply of autologous stem cells,[5] replicative senescence of stem cells on *ex vivo* expansion,[1,6,7] and low engraftment efficiency in target tissues.[8–10]

An alternative strategy for regenerating injured tissues may be to induce dedifferentiation of mature cells in the wound environment, producing a local supply of stem-like cells that can participate in healing. Such dedifferentiation occurs naturally in zebrafish heart and fin regeneration, urodele limb regeneration, and Schwann cell dedifferentiation after nerve injury.[11–18] Dedifferentiation has been studied to a limited extent in MSCs. In hMSC-derived osteoblasts and adipocytes, simple withdrawal of the biochemical inducers of ostoegenic and adipogenic differentiation is sufficient to induce down-regulation of mature tissue markers.[19] Similarly, in MSC-derived neural cells, withdrawal of extrinsic induction factors reverted cells back to a mesenchymal morphology and suppressed neural markers.[20] These dedifferentiation strategies, while successful, may not be practical for achieving cell dedifferentiation in a wound environment, where the contents of the microenvironment cannot be easily eliminated. Thus, there is a need for novel methods to modulate the terminal differentiated status of

[1]Department of Biomedical Engineering, Tufts University, Medford, Massachusetts.
[2]Department of Biology and Center for Regenerative and Developmental Biology, Tufts University, Medford, Massachusetts.

cells, which may enable us to implement dedifferentiation as a therapeutic strategy for improving tissue regeneration.

One currently unexplored strategy for modulating the differentiated state of cells is the control of endogenous bioelectric signaling. Bioelectrical signaling regulates many biological functions from the cell level to the organ level (reviewed in[21–26]), and it has been shown to be necessary and sufficient for the regeneration and patterning of large structures (limb, tail, head, and eye) in a range of vertebrate and invertebrate model organisms.[27–33] Bioelectric signaling has also been shown to regulate the behavior of mammalian stem and progenitor cells. For example, in human myoblasts, differentiation is triggered by V_{mem} hyperpolarization through the Kir2.1 channel. Hyperpolarization stimulates Ca^{2+} influx and calcineurin activation, resulting in myocyte fusion.[34–38] Hyperpolarization also induces differentiation in cardiomyocyte progenitor cells via increased intracellular Ca^{2+} and NFAT activity.[39] Similarly, late-stage maturation of neural crest cells is characterized by V_{mem} hyperpolarization and expression of K^+ and Na^+ currents.[40–43] In mouse embryonic stem cells, V_{mem} depolarization by blockade of Kv channels results in decreased proliferation, loss of pluripotency markers, and increased expression of early germ layer markers.[44] Thus, in both excitable and non-excitable cells, hyperpolarization of the transmembrane potential (V_{mem}) accompanies, and, in some cases, is required for progenitor cell differentiation and lineage restriction. In previous studies, we have shown that the resting V_{mem} level in hMSCs regulates their capacity to undergo osteogenic and adipogenic differentiation.[45] V_{mem} hyperpolarization occurs spontaneously during hMSC differentiation toward both lineages and is necessary for differentiation. Artificial induction of V_{mem} depolarization or hyperpolarization can inhibit or augment, respectively, the differentiation process. Thus, hMSC differentiation toward osteoblasts and adipocytes is functionally regulated by voltage. What is still unknown is whether this relationship holds in the reverse process: the dedifferentiation of osteoblasts and adipocytes derived from hMSCs. If bioelectric signaling, indeed, plays a role in dedifferentiation, it would be a novel and valuable tool for controlling cell plasticity for therapeutic purposes.

The goal of the present study was to determine whether voltage modulation alters the differentiated state of predifferentiated hMSCs and to identify potential mechanisms through which this effect may occur. We therefore depolarized the V_{mem} of predifferentiated hMSCs and asked (1) whether differentiation markers were down-regulated; (2) whether stemness markers were up-regulated; and (3) how the global transcriptional profile of the cells was differentially regulated in response to voltage modulation. For bone markers, we quantified gene expression of alkaline phosphatase (*ALPL*) and bone sialoprotein (*IBSP*); quantified matrix calcification; and stained samples for ALPL expression and calcium deposition. For fat markers, we quantified gene expression of peroxisome proliferator-activated receptor gamma (*PPARG*) and lipoprotein lipase (*LPL*); and stained for lipid accumulation with Oil Red O. There is currently no known stemness marker that is specific to hMSCs. However, recent reports have identified some genes that may function in maintenance of adult stem cell multipotency, lineage specific commitment, and initiation of transdifferentiation.[19,46–48] We quantified the expression of a panel of these genes to determine whether depolarized cells acquired a more stem-like transcript profile. We also examined a functional marker of stem-like behavior, the capacity for multilineage differentiation, by evaluating the ability of depolarized predifferentiated cells to differentiate along a different lineage (transdifferentiation). Finally, we profiled the global transcriptional activity of the depolarized cells to understand the mechanisms underlying the observed response to V_{mem} changes. Unlike previous microarray studies of cell response to applied electric fields and electric stimulation,[49–52] our study examines cell response to targeted manipulation of endogenous V_{mem}, providing the first comprehensive analysis of transcriptional activity triggered by directed V_{mem} changes. Using the metrics described earlier to characterize voltage-induced changes, we report that depolarization induces differentiated cells to down-regulate differentiation markers and enables them to develop a better transdifferentiated phenotype, without up-regulating any stem-associated gene transcripts. Based on the transcript profile of the depolarized cells, we also identify several voltage-responding signaling pathways of interest for further detailed study.

Materials and Methods

hMSC cultivation

Whole bone marrow aspirate from a 25 year-old healthy man was purchased from Lonza through their Research Bone Marrow Donor Program, following approved guidelines of informed consent. Aspirate was plated at a density of 10 μL of aspirate per cm^2 in control medium (DMEM with 10% fetal bovine serum (FBS), penicillin (100 U/mL), streptomycin (100 μg/mL), and 0.1 mM nonessential amino acids) supplemented with basic fibroblast growth factor (1 ng/mL) (Invitrogen). Cells were maintained in a humidified incubator at 37°C with 5% CO_2. hMSCs were isolated on the basis of their adherence to tissue culture plastic and were used for experiments between passages two and four.

Differentiation

Undifferentiated hMSCs were cultured in control medium. AD differentiation medium consisted of control medium supplemented with 0.5 mM 3-isobutyl-1-methyl-xanthine, 1 μM dexamethasone, 5 μg/mL insulin, and 50 μM indomethacin. OS differentiation medium consisted of αMEM medium supplemented with 10% FBS, penicillin (100 U/mL), streptomycin (100 μg/mL), 10 mM β-glycerophosphate, 0.05 mM L-ascorbic acid-2-phosphate, and 100 nM dexamethasone (Sigma-Aldrich). Transdifferentiation of predifferentiated osteoblasts was achieved by switching cells from OS differentiation medium to AD differentiation medium.

Depolarization of membrane potential

V_{mem} was depolarized by (1) addition of Na^+/K^+-ATPase-inhibitor ouabain (OB, 10 nM; Sigma-Aldrich) to differentiation medium or (2) elevation of extracellular K^+ by adding potassium gluconate (High K^+, HK, 40 or 80 mM; Sigma-Aldrich) to differentiation medium. Depolarization induced by these concentrations of OB and K^+ has been confirmed using voltage-sensitive dyes and/or

sharp intracellular recordings ([45]and unpublished data). These depolarizers were added at the time points indicated in the text and replenished in subsequent media changes, for the indicated durations (Figs. 1A and 3A). Briefly, OS cells were predifferentiated for 2 or 3 weeks before the addition of OB or HK for an additional 1 or 3 weeks. AD cells were predifferentiated for 2 weeks before the addition of OB or HK for an additional 1 week. In transdifferentiation studies, OB or HK were added to OS differentiation medium during Weeks 1–6 or Weeks 4–6 (constant or late depolarization, respectively), before cells were switched to AD differentiation medium during Weeks 7–8.

RNA isolation, purification, and real-time RT-PCR

RNA was isolated using Trizol (Invitrogen) following the single-step acid-phenol guanidinium method, and purified (Qiagen RNEasy kit). Reverse transcription was performed using the High-Capacity cDNA Archive kit (Applied Biosystems). Real-time RT-PCR was performed using a Stratagene Mx3000P QPCR System (Stratagene) to track differentiation markers. Osteoblast differentiation markers include *ALPL*, collagen I α1 (*COL1A1*), *IBSP*, and matrix gla protein (*MGP*). Adipogenic differentiation markers include *PPARG*, *LPL*, and fatty acid binding protein 4 (*FABP4*). Stemness markers examined include brain-derived neurotrophic factor (*BDNF*), integrin α11 (*ITGA11*), (never in mitosis gene a)-related kinase 7 (*NEK7*), neurotrimin (*NTM*), tropomyosin 1 α (*TPM1*), UDP-glucose ceramide glucosyltransferase (*UGCG*), and vascular cell adhesion molecule-1 (*VCAM1*). Primers and probes for these genes were obtained from TaqMan® Gene Expression Assay kits (Applied Biosystems). Expression levels were normalized to the housekeeping gene glyceraldehyde 3-phosphate dehydrogenase (*GAPDH*). We have previously reported PCR reaction conditions and primers.[53–55]

Calcium assay

Total calcium content was determined using the Calcium (CPC) Liquicolor Test (Stanbio Laboratory). Calcium was dissociated with trichloroacetic acid, reacted with assay solution, and measured spectrophotometrically at 575 nm (VersaMax; Molecular Devices).

ALPL assay

ALPL activity was assessed by detecting the hydrolysis of p-nitrophenyl phosphate to p-nitrophenol. Cultured cells were lysed with 0.2% v/v Triton X-100 in 5 mM $MgCl_2$, and incubated with substrate in 2-amino-2-methyl-1-propanol buffer (Sigma-Aldrich). The hydrolysis reaction was stopped by 0.2 M NaOH and measured spectrophotometrically at 405 nm.

Oil Red O staining

Cells were fixed in 10% formalin for 1 h, washed with 60% isopropanol, and air dried. Oil Red O working solution (60%) was prepared from a stock solution (0.7 g Oil Red O in 200 mL isopropanol) and filtered. Cells were stained for 45 min, washed five times with distilled water, and imaged at room temperature with an inverted microscope (Axiovert S100; Carl Zeiss, Inc.) equipped with Zeiss A-Plan 10×(NA 0.25) and LD A-Plan 32×(0.40) objectives. Images captured by a Sony Exwave HAD CCD camera were acquired using ImageJ software (NIH). Photoshop software (Adobe Systems, Inc.) was used to adjust brightness and contrast levels over the entire image. Oil Red O was eluted with isopropanol for 1 h and measured spectrophotometrically at 500 nm.

ALPL and Alizarin Red staining

Cells were fixed in 1% formaldehyde and stained for ALPL using the Leukocyte ALP assay kit (Sigma-Aldrich). Cells were then stained with Alizarin Red to visualize calcified mineral deposition and imaged as above.

Statistics

Data are reported as means ± standard error. One-way ANOVA statistical analysis was performed in experiments with more than two groups, followed by the Tukey–Kramer *post-hoc* test. In bar graphs, means labeled with the same letter are not significantly different from one another (Tukey–Kramer, $p > 0.05$). Student's *t*-test analysis was performed in experiments comparing two groups, with results considered significant if $p < 0.05$.

Microarray

RNA was isolated as described earlier with the addition of an on-column DNase treatment performed during RNA purification. RNA quality was evaluated on an Agilent Bioanalyzer. cDNA reverse transcription; cDNA purification; *in vitro* transcription of cRNA; and microarray hybridization, staining, and scanning were performed by the Yale Center for Genomic Analysis. Illumina Human WG6 v3 Expression BeadChips were used. OB-treated, HK-treated, and untreated OS groups: $n = 3$. UN group: $n = 2$.

Microarray data analysis

Bioconductor software packages were used to perform data analysis. Variance stabilizing transformation and quantile normalization were performed using the *lumi* package.[56,57] Hierarchical clustering was performed with the Ward method, using the Pearson correlation as the distance metric. Principal component analysis (PCA) was performed, and genes of interest were ranked according to loading values. Linear modeling was performed for differential expression analysis using the *limma* package.[58] Log2-fold gene expression changes were plotted as heatmaps using the packages *gplots* and *RColorBrewer*. *p*-Values were adjusted according to the Benjamini–Hochberg method and considered significant if *p*-value < 0.01. The *GOstats* package was used to perform hypergeometric testing on Gene Ontology (GO) terms.[59] *p*-Values were adjusted for multiple testing and considered significant if $p < 0.01$. The online tool REVIGO was used to reduce redundancy of GO terms and display results.[60] Gene set enrichment analysis (GSEA) was used to evaluate whether the canonical pathways gene sets from the Molecular Signatures Database were statistically different between groups.[61,62] Results were ranked by Normalized Enrichment Score and were considered significant if false discovery rate < 0.05.

Results

HK suppresses mature phenotype of predifferentiated osteoblasts and adipocytes

Previous studies indicate that V_{mem} depolarization affects the differentiation process of hMSCs.[45] In the present study, we investigated whether V_{mem} depolarization affects the differentiated state of hMSC-derived cells after they have been predifferentiated to osteoblasts or adipocytes. Depolarized cells were compared with predifferentiated cells switched to control medium (CON) (Fig. 1A), which is the standard method that is currently employed to induce de-differentiation.[19,20,63] In our predifferentiated hMSCs, CON treatment resulted in a decreased osteoblast or adipocyte phenotype (Fig. 1B–L), although cells did not completely revert to the undifferentiated state.

To investigate the effect of depolarization on the osteoblast phenotype, hMSCs were predifferentiated toward the osteoblast lineage for 2 weeks and subsequently treated for 1 week with either 10 nM OB or 80 mM HK, which were added to the osteogenic medium. *IBSP* expression was reduced in OB- and HK-treated cells (11.3-fold, $p < 0.001$; 6.3-fold, $p < 0.01$, respectively) compared with untreated osteoblasts, and was not statistically different from CON-treated or undifferentiated cells (Fig. 1C). ALPL activity levels in OB- and HK-treated cells were reduced 2.1-fold ($p < 0.001$) and 1.5-fold ($p < 0.01$), respectively, compared with untreated osteoblasts, and was not statistically different from osteoblasts that were de-differentiated by CON medium (Fig. 1B). While OB treatment did not affect total calcium, HK treatment significantly down-regulated calcification compared with untreated osteoblasts ($4.7 \pm 0.9\,\mu g$ vs. $25.0 \pm 0.9\,\mu g$, $p < 0.001$) (Fig. 1D). Calcium levels were reduced more effectively by HK depolarization than by CON medium ($p < 0.05$), and calcium levels of HK-treated cells were similar to undifferentiated cells. hMSCs subjected to longer periods of osteogenic predifferentiation and depolarization (3 weeks of differentiation, 3 weeks of depolarization with 40 mM HK, Fig. 1A) exhibited similar behavior. HK and CON treatments suppressed calcium levels compared with untreated osteoblasts ($213.7 \pm 29.2\,\mu g$ and $210.1 \pm 16.9\,\mu g$, respectively, vs. $365.3 \pm 11.7\,\mu g$, $p < 0.001$, Fig. 1M). Alizarin Red staining also showed lower mineral deposition in both HK- and CON-treated groups (Fig. 1O, Q, respectively) compared with untreated osteoblasts (Fig. 1P). OB, however, did not significantly reduce calcium levels ($342.9 \pm 8.3\,\mu g$ vs. $365.3 \pm 11.7\,\mu g$, $p > 0.05$, Fig. 1M, N). Depolarization by HK can, therefore, reduce bone markers despite the presence of osteogenic factors and can do so more effectively than withdrawal of these osteogenic factors.

To examine whether adipocytes exhibit the same sensitivity to depolarization, hMSCs were predifferentiated toward adipocytes for 2 weeks and subsequently treated for 1 week with HK in AD differentiation medium. Compared with untreated adipocytes, HK treatment down-regulated expression of *PPARG* (5.8-fold, $p < 0.001$) and *LPL* (374.8-fold, $p < 0.001$), which are early and late markers of AD differentiation, respectively (Fig. 1E, F). Oil Red O staining confirmed that HK treatment reduced lipid accumulation (Fig. 1G, H). Depolarization, therefore, suppresses, but does not completely eliminate the mature adipocyte phenotype.

Depolarization does not induce re-expression of genes associated with stem state

Since HK treatment caused predifferentiated osteoblasts and adipocytes to lose expression of mature tissue markers, we then asked whether the depolarized cells had reverted to a more stem-like phenotype. We quantified expression of a panel of genes related to maintenance of stem cell multipotency, lineage commitment, and initiation of transdifferentiation in our depolarized cells.[19,46–48] All but one of the genes (protein tyrosine phosphatase receptor F, not shown) behaved as a stem marker (Fig. 2A–N). HK depolarization did not up-regulate expression of the stem-associated genes during either OS or AD differentiation (Fig. 2A–N). HK treatment, therefore, did not cause cells to re-express genes associated with the stem state, despite the loss of osteoblast and adipocyte markers.

Depolarization may prime osteoblasts, but not adipocytes, for transdifferentiation

Since depolarization did not cause the cells to re-express genes associated with the stem state, we asked whether the treatment might instead prime the cells for differentiation along a different lineage (transdifferentiation). We quantified expression of adipogenic markers in the depolarized osteoblasts, as well as osteogenic markers in the depolarized adipocytes (Fig. 2O–U). In HK-treated osteoblasts, expression of the adipogenic marker *FABP4* was 1.9-fold higher than untreated osteoblasts ($p < 0.05$, Fig. 2O); while expression of *PPARG* and *LPL* showed higher trends, though not statistically significant ($p > 0.05$, Fig. 2P, Q). In contrast, HK-treated adipocytes demonstrated an overall suppression of the osteogenic direction: 31.6-fold decreased *ALPL*, 12.5-fold decreased *COL1A1*, 310.8-fold decreased *IBSP*, and 11.1-fold decreased *MGP* expression compared with untreated adipocytes ($p < 0.001$, Fig. 2R–U). Depolarized adipocytes, therefore, down-regulate osteogenic gene expression, while depolarized osteoblasts exhibit adipogenic gene expression trends that are potentially favorable for transdifferentiation.

Depolarized osteoblasts retain the capacity to transdifferentiate to adipocytes

Since depolarized osteoblasts showed potential to transdifferentiate, we asked whether these cells could indeed transdifferentiate when stimulated with adipogenic medium. We differentiated hMSCs toward osteoblasts for 6 weeks before transdifferentiating them toward adipocytes for 2 weeks (Fig. 3A). Before transdifferentiation, cells were subjected to constant depolarization (40 mM HK, Weeks 1–6), late depolarization (40 mM HK, Weeks 4–6), or CON treatment (Weeks 4–6).

Under normal conditions, hMSC-derived osteoblasts maintained the ability to differentiate along the adipogenic lineage despite having already progressed down the osteoblastic lineage. Transdifferentiated cells decreased calcification between Weeks 6 and 8 ($37.6 \pm 1.4\,\mu g$ vs. $53.6 \pm 0.3\,\mu g$, $p < 0.01$, Fig. 3B), expressed several adipogenic transcripts (*PPARG, LPL, FABP4*, Fig. 3D–F), and accumulated a similar amount of lipid as untreated adipogenic cells (Fig. 3C). Many adipocytes had an elongated, spindle-like morphology that was more reminiscent of undifferentiated hMSCs than adipocytes (Fig. 3I). After CON pretreatment, transdifferentiated cells also expressed *PPARG*, *LPL*, and *FABP4*

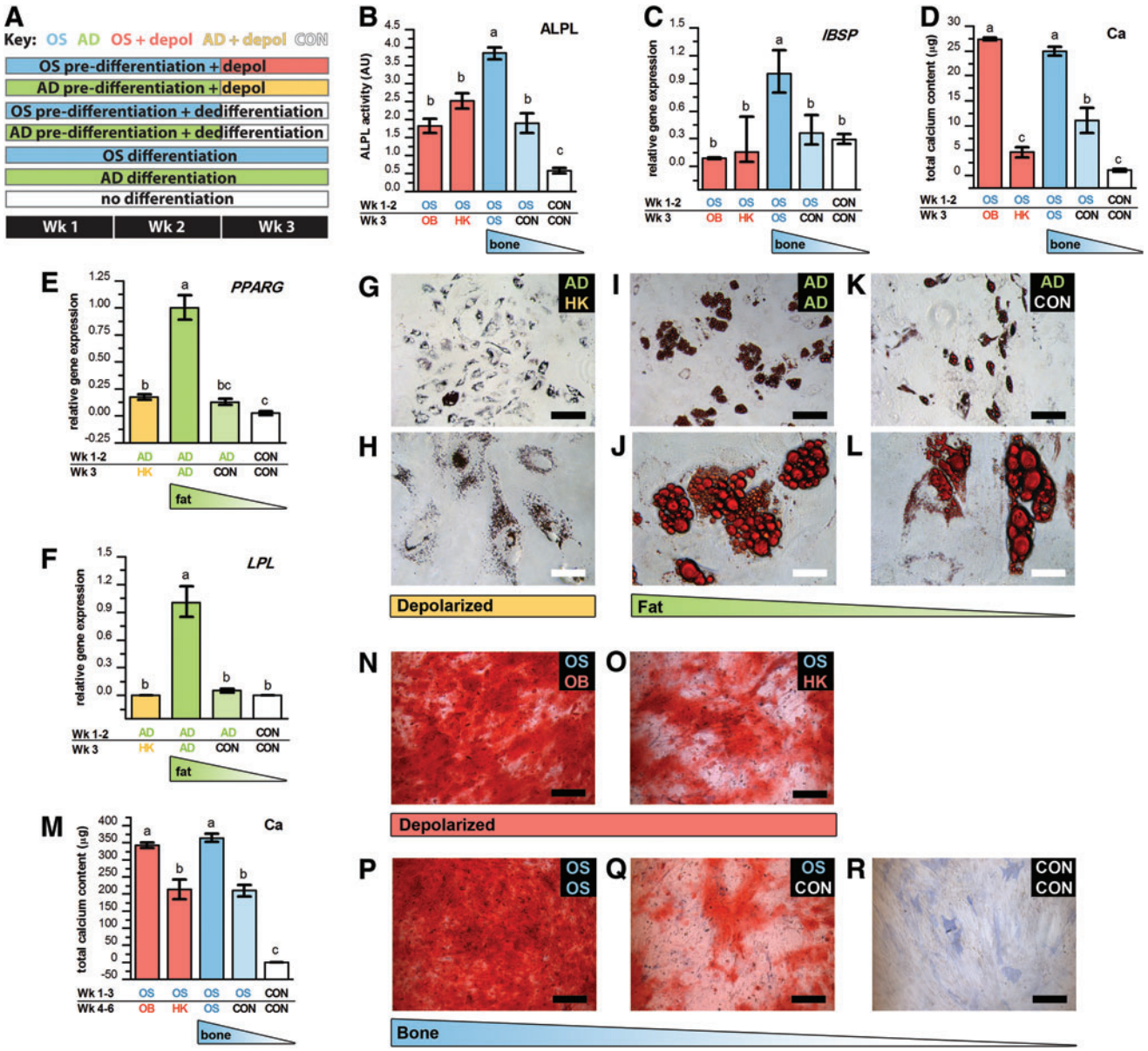

FIG. 1. Depolarization of predifferentiated hMSCs causes loss of osteoblast and adipocyte phenotypes. **(A)** Schematic of predifferentiation and depolarization treatments. **(B)** ALPL activity in predifferentiated osteoblasts was decreased by OB, HK (80 mM K^+), and CON treatments compared with untreated osteoblasts. Data represent mean enzyme activity (AU) ± standard error, $n = 4$. **(C)** *IBSP* gene expression in predifferentiated osteoblasts was lowered by OB, HK, and CON treatments compared with untreated osteoblasts. Data points are mean relative expression ± standard error, $n = 4$–5. **(D)** Calcification was lowered by HK and CON treatments, but not by OB, compared with untreated osteoblasts. Data points are mean calcium mass (μg) ± standard error, $n = 6$. **(E, F)** *PPARG* and *LPL* gene expression was lowered by HK and CON treatments compared with untreated adipocytes. Data points are mean relative expression ± standard error, $n = 5$–6. **(G-L)** Oil Red O staining of lipids in HK-treated **(G, H)**, CON-treated **(K, L)**, and untreated **(I, J)** adipocytes. **(M)** Calcification in predifferentiated osteoblasts treated for 3 weeks with HK (40 mM K^+) and CON was reduced compared with untreated osteoblasts. Data points are mean calcium mass (μg) ± standard error, $n = 6$. **(N-R)** ALPL (blue) and Alizarin Red (red) staining of osteoblasts in OB-treated **(N)**, HK-treated **(O)**, CON-treated **(Q)**, and untreated **(P)** osteoblasts, and undifferentiated cells **(R)**. Black scale bars = 200 μm. White scale bars = 50 μm. Different letters over bar graphs represent statistically different groups as determined by one-way ANOVA and the Tukey–Kramer *post-hoc* test, $p < 0.05$. hMSCs, human mesenchymal stem cells; OS, osteogenic medium; AD, adipogenic medium; depol, depolarizing agents; OB, 10 nM ouabain; HK, high K^+; CON, control medium; ALPL, alkaline phosphatase; IBSP, bone sialoprotein; PPARG, peroxisome proliferator-activated receptor γ; LPL, lipoprotein lipase. Color images available online at www.liebertpub.com/tea

(Fig. 3D–F); adopted a typical rounded morphology (Fig. 3H); and accumulated more lipid than the transdifferentiated group and the untreated adipogenic group ($p < 0.001$, Fig. 3C).

Depolarized cells did not exhibit a statistically significant decrease in total calcium content on transdifferentiation between Week 6 and Week 8 (Fig. 3B), which may be because HK had already significantly lowered the amount of total calcium at Week 6. *PPARG*, *LPL*, and *FABP4* gene expression in HK-treated cells was similar to that of directly transdifferentiated cells (Fig. 3D–F). Oil Red O staining of lipid droplets showed similar lipid accumulation in late-depolarized cells and directly transdifferentiated cells (Fig. 3C). In contrast to the spindle-like morphology obtained with directly transdifferentiated cells, adipocytes produced from both depolarized populations adopted a rounded morphology (Fig. 3J–K) that was more typical of normal hMSC-derived adipocytes (Fig. 3G). Altogether, these results show that depolarized hMSC-derived cells retain their lineage plasticity and achieve better morphological outcomes after transdifferentiation than nondepolarized cells.

Microarray analysis of hMSCs depolarized after predifferentiation

To better understand the mechanisms mediating voltage signaling, we performed microarray analysis on osteoblasts depolarized after predifferentiation. Osteoblasts were predifferentiated for 3 weeks and subsequently treated with 10 nM OB or 40 mM HK in differentiation medium for an additional 3 weeks. For comparison, other samples were maintained in osteogenic medium (OS) or kept undifferentiated (UN) for the entire 6 weeks. Hierarchical clustering of the data (Fig. 4A) revealed that depolarized groups (OB and HK) were the most similar, despite their different effects on the differentiated state of the hMSC-derived osteoblasts. Furthermore, both the depolarized groups were more similar to the OS group than to the UN group.

For further data analysis, we chose to focus on the differences between the OB, HK, and OS groups. From PCA, the first two principal components (PC) best represented the inter-group variance while minimizing intra-group variance among replicates (Fig. 4B). Projection onto PC 1 exhibits a clustering pattern that is similar to hierarchical clustering. Projection onto PC 2 separates the HK group from the others. Genes with the highest loading values in PC1 and 2 were largely related to mitochondria, metabolism, cell structure, adhesion, migration, and remodeling (Table 1).

Using a linear modeling approach, we quantified log-fold differences in gene expression between the OS group and the depolarized groups. Table 2 shows the top differentially expressed genes, ranked according to their moderated F-statistic, and Figure 5A shows a clustered heatmap of these genes. We performed hypergeometric testing on the GO terms associated with the genes to understand the biological processes that they represent, and used the tool ReVIGO to visualize the results (Fig. 4C).[60] Similar to the PCA results, a number of genes related to metabolism and cell migration, adhesion, and remodeling are highly differentially expressed. In addition, the data implicate the participation of major signaling pathways, including Rho (*ARHGDIB*), G-protein (*RGS*), TNF (*C1QTNF*), Wnt (*SFRP2, SFRP4*), platelet-derived growth factor (*PDGFRL*), and interleukin (*IL8*) signaling pathways.

We sought to identify genes that could be responsible for the opposite effects of OB and HK on osteoblast differentiated state by filtering for genes responding in opposite directions to OB versus HK treatment (Table 3 and Fig. 5B). Hypergeometric testing revealed several overrepresented GO terms, including translational elongation; translation; muscle organ development; cardiac muscle tissue development; and antigen processing and presentation of peptide antigen via MHC class I.

To identify pathways, rather than individual genes, enriched by depolarization, we performed GSEA on OB and HK groups versus OS group (Table 4). Of the top HK-enriched pathways, most are involved in cell cycle regulation; protein degradation and proteasome function; mRNA processing; and metabolism. Many of the pathways enriched in the HK group are also enriched in the OB group. The OB group also is enriched for insulin-related pathways. The Wnt pathway, identified by differential-expression analysis as a potential pathway of interest, is enriched in both groups. Comparing the HK and OB groups with one another yielded enriched pathways that are associated with muscle function; semaphorin and Rho signaling; and extracellular matrix and integrin interactions (Table 5). We also identified the leading edge genes that are most responsible for the enrichment results. Most leading edge genes in the OB versus OS and HK versus OS comparisons are related to proteasome, splicing, and ribosome functions (Table 6). The leading edge genes in the OB versus HK comparison are largely related to cell structure and adhesion (Table 7).

Discussion

Bioelectric signaling regulates differentiation in a number of excitable and nonexcitable stem and progenitor cells, but its effects on the differentiated state of mature, nonexcitable somatic cells has not yet been well characterized. The goal of this study was to determine how predifferentiated hMSCs respond to modulation of their V_{mem}, in particular (1) whether their differentiated state changes on stimulation; (2)

FIG. 2. HK-depolarization does not induce re-expression of stem-associated markers, but may prime predifferentiated osteoblasts for transdifferentiation to adipocytes. Gene expression of brain-derived neurotrophic factor (*BDNF*), integrin α11 (*ITGA11*), (never in mitosis gene a)-related kinase 7 (*NEK7*), neurotrimin (*NTM*), tropomyosin 1 α (*TPM1*), UDP-glucose ceramide glucosyltransferase (*UGCG*), and vascular cell adhesion molecule-1 (*VCAM1*) in predifferentiated osteoblasts **(A–G)** and adipocytes **(H–N)** treated with HK or CON. Gene expression of *FABP4*, *LPL*, and *PPARG* in predifferentiated osteoblasts **(O–Q)** treated with HK or CON. Gene expression of *COL1A1*, *ALPL*, *IBSP*, and *MGP* in predifferentiated adipocytes **(R–U)** treated with HK or CON. Data points are mean relative expression ± standard error, $n = 4–6$. Different letters over bar graphs represent statistically different groups as determined by one-way ANOVA and the Tukey–Kramer *post-hoc* test, $p < 0.05$. HK, high K^+ (80 mM K^+); COL1A1, collagen type I α1; MGP, matrix gla protein; FABP4, fatty acid binding protein-4. Color images available online at www.liebertpub.com/tea

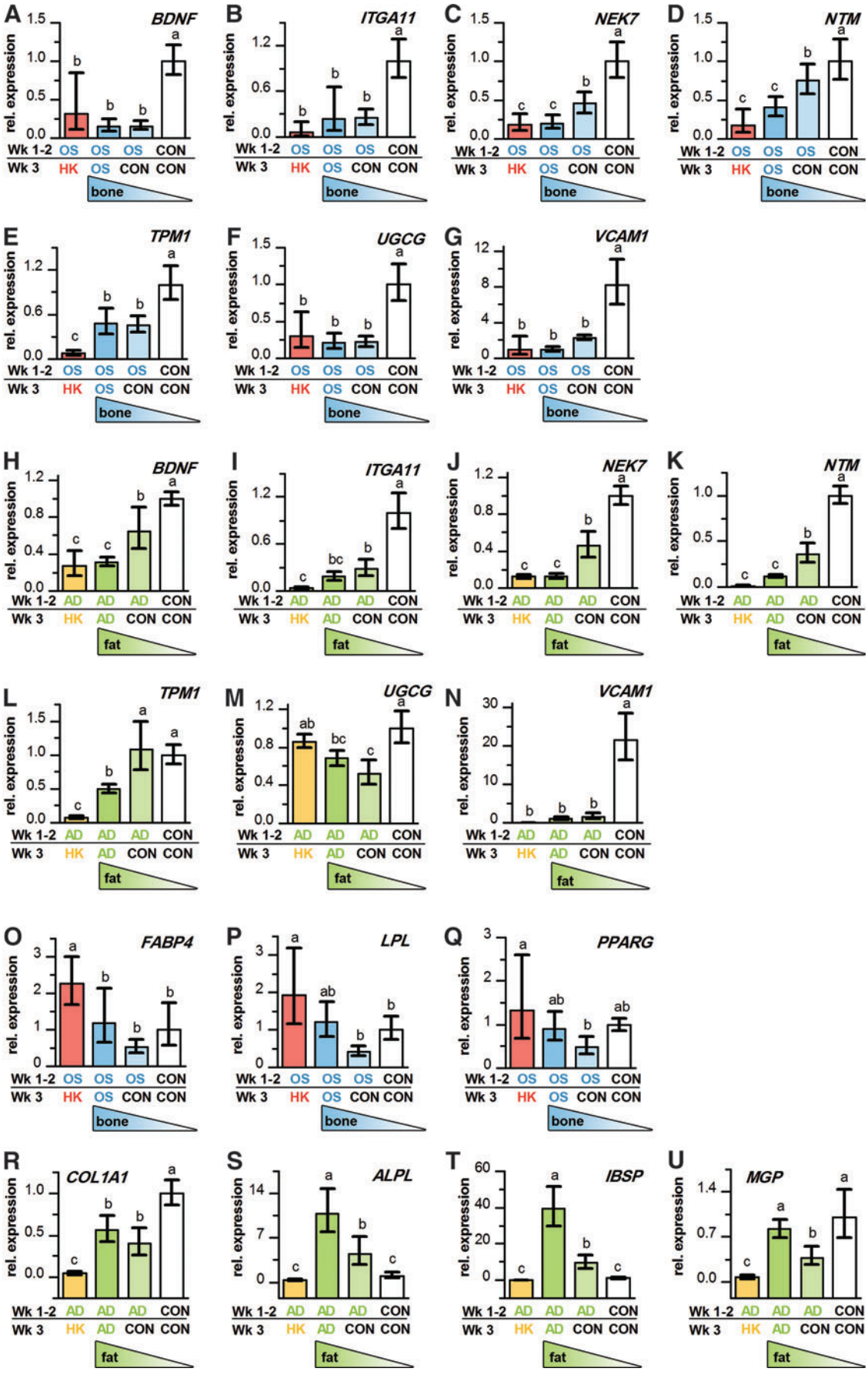
A BDNF
B ITGA11
C NEK7
D NTM
E TPM1
F UGCG
G VCAM1
H BDNF
I ITGA11
J NEK7
K NTM
L TPM1
M UGCG
N VCAM1
O FABP4
P LPL
Q PPARG
R COL1A1
S ALPL
T IBSP
U MGP
rel. expression
Wk 1-2 OS OS OS CON
Wk 3 HK OS CON CON
bone
Wk 1-2 AD AD AD CON
Wk 3 HK AD CON CON
fat

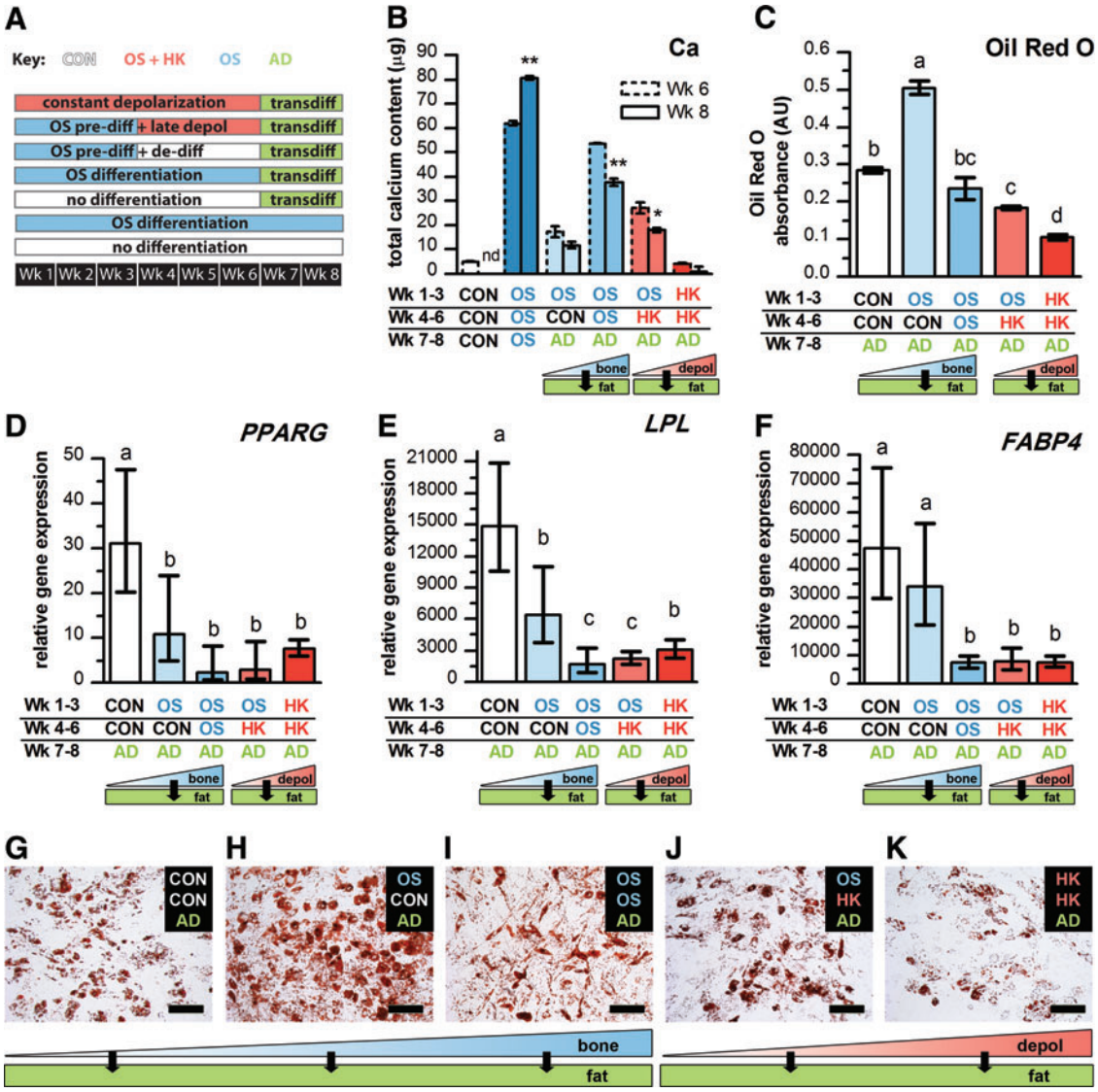

FIG. 3. Osteoblasts treated with constant or late HK depolarization are capable of adipogenic transdifferentiation, and thus retain lineage plasticity in the adipogenic direction. **(A)** Schematic showing different pretreatments before adipogenic transdifferentiation. **(B)** Calcium content at Weeks 6 and 8, immediately before and after transdifferentiation. Data points are total calcium mass (µg) ± standard error, $n = 4$–6. Significance was measured using the student's *t*-test between Week 6 and Week 8 data, and is indicated with *($p < 0.05$) and **($p < 0.001$). **(C)** Oil Red O staining of transdifferentiated cells was quantified in nondepolarized osteoblasts (OS-OS-AD), late-depolarized osteoblasts (OS-HK-AD), constant-depolarized osteoblasts (HK-HK-AD), CON-treated osteoblasts (OS-CON-AD), and untreated adipocytes (CON-CON-AD). Data points are absorbance values (AU) ± standard error, $n = 4$. **(D–F)** *PPARG*, *LPL*, and *FABP4* gene expression was measured in transdifferentiated cells and untreated adipocytes. Data points are mean relative expression ± standard error, $n = 4$–5. Different letters over bar graphs represent statistically different groups as determined by one-way ANOVA and the Tukey–Kramer *post-hoc* test, $p < 0.05$. **(G–K)** Oil Red O staining of untreated adipocytes **(G)** and transdifferentiated cells derived from constant-depolarized **(K)**, late-depolarized **(J)**, Con-treated **(H)**, and untreated **(I)** osteoblasts. Scale bars = 200 µm. HK, high K^+ (40 mM K^+). Color images available online at www.liebertpub.com/tea

whether their lineage plasticity is affected by stimulation; and (3) which signaling pathways mediate their V_{mem} response.

In this study, depolarization of hMSC-derived osteoblasts and adipocytes by treatment with HK reduced expression of markers of the mature phenotype. Osteoblasts and adipocytes derived from hMSCs have been previously shown to dedifferentiate on withdrawal of osteogenic or adipogenic stimulants from their media.[19] In our studies, depolarization induced reversal of the mature phenotype even in the presence of differentiation stimulants in the media, suggesting that V_{mem} signals may override the biochemical signals that promote differentiation. This depolarization-induced phenotype suppression was confirmed in follow-up studies using hMSCs from two additional bone marrow donors (data not shown). Although hMSCs from all three bone marrow sources demonstrated donor-dependent variability in baseline differentiation levels, as has been previously

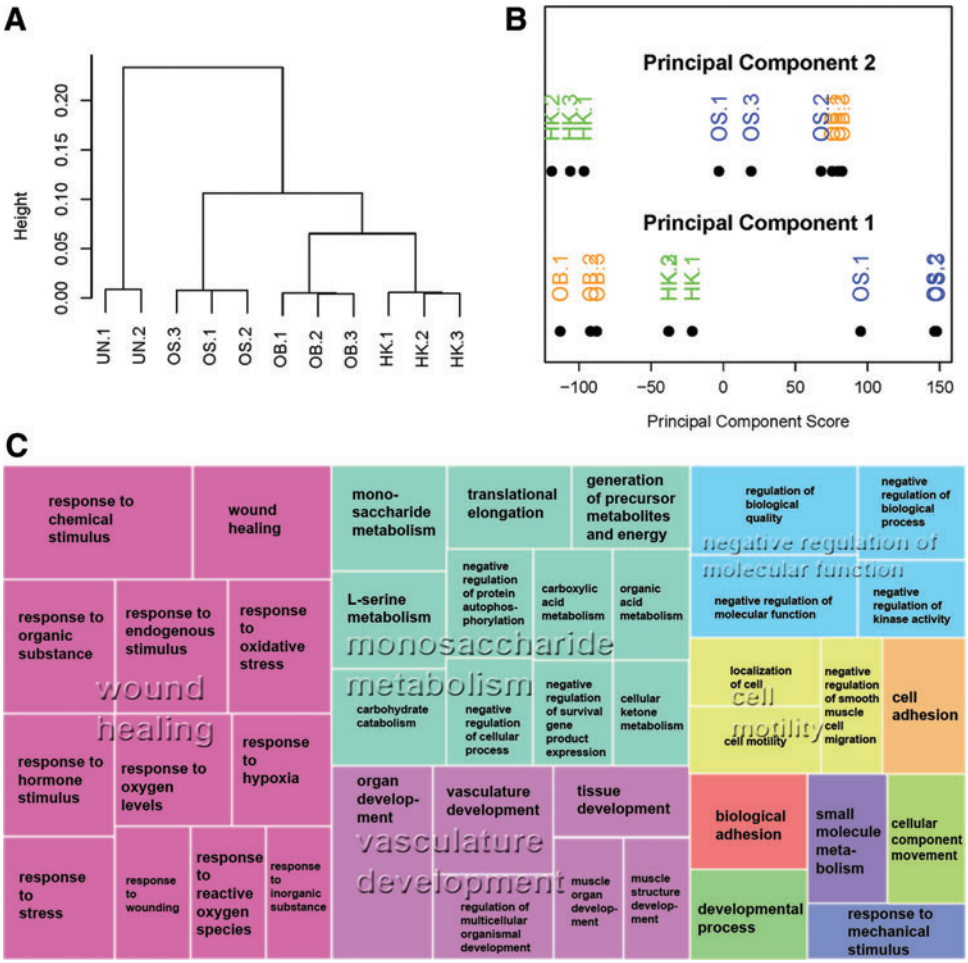

FIG. 4. Genome-wide expression analysis results summarized by clustering, principal component analysis (PCA), and hypergeometric testing of Gene Ontology (GO) terms. **(A)** Hierarchical clustering of microarray transcript data from undifferentiated (UN), untreated osteogenic (OS), ouabain-treated (OB), and high-K^+-treated (HK, 40 mM K^+) groups. **(B)** One-dimensional projections of principal components 1 and 2 (PC1 and PC2) from PCA analysis of microarray transcript data. **(C)** Visualization of overrepresented GO terms describing the functions of differentially expressed genes. Figure adapted from output of REVIGO analysis[60] (See Materials and Methods section for details). OB, ouabain-treated (10 nM); HK, high-K^+-treated (40 mM K^+). Color images available online at www.liebertpub.com/tea

reported for bone marrow-derived hMSCs,[64,65] all donors exhibited the same response to voltage modulation: decreased osteogenic and adipogenic markers compared with untreated cells from their respective donors. This consistency of response confirms that hMSC response to voltage modulation is a reproducible phenomenon among donors. V_{mem}, therefore, plays a functional role in the maintenance of differentiated state, and it may be a novel control point for fine tuning the status of mature cells.

Although markers of the osteoblast and adipocyte phenotypes were reduced on depolarization, they were not lost completely. For example, ALPL activity and calcification in predifferentiated osteoblasts was reduced on depolarization compared with untreated osteoblasts, but was still greater than that of undifferentiated hMSCs. Gene expression in depolarized, predifferentiated adipocytes was significantly reduced, but cells still accumulated small lipid droplets. These data indicate that depolarized cells did not completely revert to the undifferentiated state. It is possible that cells in this partially differentiated state resemble hMSCs which are at more immature stages along the path of differentiation toward bone and fat. This would need to be clarified with further studies comparing depolarized cells with hMSCs differentiated for different periods of time.

We also sought to determine whether depolarized cells re-expressed any markers of the stem phenotype of hMSCs. Currently, hMSCs are identified by their expression of a panel of cell surface markers. However, it is generally unclear whether these markers are specific to the undifferentiated, stem state. One group reports that high *VCAM1* expression is characteristic of the undifferentiated, but not differentiated, hMSC state.[48] Others have exploited microarray technology to identify genes associated with maintenance of adult stem cell multipotency, lineage-specific commitment, and initiation of transdifferentiation.[19,46,47] Many of these genes also behaved as stemness markers in our system. When predifferentiated hMSCs were depolarized, they did not significantly up-regulate expression of any of these putative stem-associated genes, despite reduction of the mature phenotype.

Depolarized osteoblasts were, however, capable of adipogenic transdifferentiation, indicating that lineage plasticity in the OS-to-AD direction is preserved during V_{mem} modulation. Moreover, depolarized cells had a rounded morphology that was more similar to normal hMSC-derived adipocytes, as opposed to the elongated morphology of the directly transdifferentiated cells. Interestingly, osteogenic cells treated with control medium exhibited better adipogenic potential than undifferentiated cells. Osteogenesis and adipogenesis are usually reported to be mutually inhibitory.[66–73] However, we hypothesize that exposing cells to a period of osteogenic predifferentiation may activate

Table 1. Principal Component Analysis Results: Genes with Highest Loadings in Principal Components 1 and 2 (PC 1, PC 2)

PC 1		PC 2	
Symbol	*Gene Name*	*Symbol*	*Gene Name*
MRP63[a]	Mitochondrial ribosomal protein 63	*MAFF*	V-mafmusculoaponeurotic fibrosarcoma oncogene homolog F (avian)
DAB2	Disabled homolog 2, mitogen-responsive phosphoprotein (Drosophila)	*SLC25A28*[a]	Solute carrier family 25, member 28
TIAM2[b]	T-cell lymphoma invasion and metastasis 2	*C15orf52*	Chromosome 15 open reading frame 52
CDC42EP3[b]	CDC42 effector protein (Rho GTPase binding) 3	*ACTC1*[b]	Actin, alpha, cardiac muscle 1
VSTM2L	V-set and transmembrane domain containing 2 like	*PTGES*	Prostaglandin E synthase
CYB5R1[a]	Cytochrome b5 reductase 1	*CNN1*[b]	Calponin 1, basic, smooth muscle
PLAT[b]	Plasminogen activator, tissue	*COMMD10*	COMM domain containing 10
PYROXD2[a]	Pyridine nucleotide-disulphide oxidoreductase domain 2	*CFH*	Complement factor H
RPS7	Ribosomal protein S7	*SNRNP70*	Small nuclear ribonucleoprotein 70 kDa (U1)
FIBP	Fibroblast growth factor (acidic) intracellular binding protein	*EBPL*	Emopamil binding protein-like
ZNF135	Zinc finger protein 135	*SDHC*[a]	Succinate dehydrogenase complex, subunit C, integral membrane protein, 15 kDa
RARS2[a]	Arginyl-tRNA synthetase 2, mitochondrial	*FAM109B*	Family with sequence similarity 109, member B
FRMD4A	FERM domain containing 4A	*ATL1*	Atlastin GTPase 1
NOTCH3	Notch 3	*UBR3*	Ubiquitin protein ligase E3 component n-recognin 3 (putative)
CLDN7	Claudin 7	*HSPB1*	Heat shock 27 kDa protein 1
TM6SF1	Transmembrane 6 superfamily member 1	*VCAM1*[b]	Vascular cell adhesion molecule 1
KCNJ15	Potassium inwardly-rectifying channel, subfamily J, member 15	*MRRF*[a]	Mitochondrial ribosome recycling factor
C20orf11	Chromosome 20 open reading frame 11	*CKS1B*	CDC28 protein kinase regulatory subunit 1B
HSF2BP	Heat shock transcription factor 2 binding protein	*RAB7B*	RAB7B, member RAS oncogene family
POMGNT1	Protein O-linked mannose beta1,2-N-acetylglucosaminyltransferase	*IFFO1*[b]	Intermediate filament family orphan 1

[a]Genes related to metabolism and mitochondria.
[b]Genes related to cell structure, adhesion, migration, and remodeling.

signaling pathways or may initiate secretion of cytokines that have both pro-osteogenic and pro-adipogenic effects. For example, bone morphogenetic proteins,[74–79] fibroblast growth factors,[80–83] and insulin-like growth factor-1[84–86] can positively regulate both bone and fat lineages. In addition, Smad and p38-MAPK signaling events promote both osteogenesis and adipogenesis.[87–89] Cytokine secretion or pathway activation may play a pro-osteogenic role during predifferentiation, but may switch to a pro-adipogenic role upon subsequent transdifferentiation. Related evidence suggests that osteogenic and adipogenic differentiation may not be exclusively reciprocal, but instead may occur in parallel until late stages of differentiation.[90] Committed osteoblasts express adipogenic markers to a greater extent than uncommitted cells, and osteogenic differentiation is accompanied by up-regulation of adipogenic markers in addition to osteogenic markers.[90] Our cells may similarly up-regulate both osteogenic and adipogenic markers during the predifferentiation stage, thus setting the stage for improved transdifferentiation when given appropriate adipogenic stimuli. Inserting an intermediate phase of dedifferentiation, whether by control medium or by depolarization, could serve to down-regulate expression of mature tissue markers before transdifferentiation. These data suggest that transdifferentiation may be improved by pre-exposure to treatments that reduce the mature osteoblastic phenotype. In situations in which it may not be feasible to remove biochemical inducers from the local cell environment (e.g., *in vivo*), an alternative strategy for transdifferentiation may be to prime cells by V_{mem} depolarization.

Collectively, these data raise an interesting question with regard to the exact state of depolarized differentiated hMSCs. Depolarization causes the cells to reduce their expression of mature tissue markers and to improve their transdifferentiation capacity, which might suggest a degree of reprogramming, as they lose their differentiated phenotype and gain stem cell-like behavior. However, the depolarized cells possess an overall genetic signature that is more similar to differentiated than undifferentiated cells and do not up-regulate stem-associated markers. Since the depolarized phenotype does not completely recapture the stem cell phenotype, depolarization does not appear to trigger a full reprogramming event. Instead, we hypothesize that the depolarized cells have been rolled back to an intermediate

Table 2. Top 50 Differentially Expressed Genes in OB and HK Groups

Gene symbol	*Gene name*	*Log-fold change in OB*	*Log-fold change in HK*	*F-statistic*	*Adjusted p-value*
MYH11[a]	Myosin, heavy chain 11, smooth muscle	−1.29	1.87	1374.81	2.2E-14
ACTG2[a]	Actin, gamma 2, smooth muscle, enteric	−2.20	0.44	1080.05	6.7E-14
PHGDH[b]	Phosphoglycerate dehydrogenase	−0.78	−2.63	1042.89	6.7E-14
STC1	Stanniocalcin 1	2.33	0.08	982.84	7.6E-14
SPARCL1	SPARC-like 1 (hevin)	−2.59	−1.30	962.10	7.6E-14
PSAT1[b]	Phosphoserine aminotransferase 1	−1.23	−2.57	915.94	9.3E-14
PIP	Prolactin-induced protein	1.36	−1.16	864.08	1.3E-13
CORIN	Corin, serine peptidase	−2.26	−0.58	781.81	2.4E-13
HOPX	HOP homeobox	−1.96	0.15	772.65	2.4E-13
ASNS[b]	Asparagine synthetase (glutamine-hydrolyzing)	−1.35	−2.49	763.37	2.4E-13
NPTX1	Neuronal pentraxin I	−0.67	1.53	722.30	3.3E-13
ANGPTL2	Angiopoietin-like 2	2.29	0.98	690.12	3.8E-13
SCG2	Secretogranin II	2.09	0.37	688.71	3.8E-13
SPARCL1	SPARC-like 1 (hevin)	−2.17	−0.91	666.27	4.5E-13
C10orf10	Chromosome 10 open reading frame 10	−1.44	0.66	663.03	4.5E-13
PTGDS	Prostaglandin D2 synthase 21 kDa (brain)	−2.00	−0.30	652.97	4.7E-13
CDO1[b]	Cysteine dioxygenase, type I	1.98	1.82	646.84	4.8E-13
AKR1C4[b]	Aldo-keto reductase family 1, member C4	2.15	1.23	620.51	6.3E-13
C13orf15	Chromosome 13 open reading frame 15	−2.03	−1.69	615.15	6.4E-13
MMP7	Matrix metallopeptidase 7 (matrilysin, uterine)	−2.05	−0.63	608.05	6.7E-13
CDO1	Cysteine dioxygenase, type I	1.83	1.70	598.87	7.2E-13
COL7A1[a]	Collagen, type VII, alpha 1	−1.86	−1.56	554.34	1.3E-12
AKR1C2[b]	Aldo-keto reductase family 1, member C2	2.21	1.03	538.38	1.5E-12
ARHGDIB	Rho GDP dissociation inhibitor (GDI) beta	−1.95	−1.15	532.99	1.6E-12
RGS4	Regulator of G-protein signaling 4	1.02	−0.83	493.43	2.8E-12
ACTC1[a]	Actin, alpha, cardiac muscle 1	−0.27	1.45	470.89	3.8E-12
C1QTNF1	C1q and tumor necrosis factor related protein 1	2.02	0.72	470.82	3.8E-12
LBH	Limb bud and heart development homolog (mouse)	1.50	1.69	465.48	3.9E-12
KCNMB1	Potassium large conductance calcium-activated channel, subfamily M, beta member 1	−1.46	0.19	464.91	3.9E-12
SFRP4	Secreted frizzled-related protein 4	1.80	0.97	461.95	3.9E-12
PCK2[b]	Phosphoenolpyruvate carboxykinase 2 (mitochondrial)	−1.49	−1.61	458.26	4.1E-12
PDGFRL	Platelet-derived growth factor receptor-like	1.75	0.80	433.77	6.0E-12
IL8	Interleukin 8	−0.53	−1.74	431.32	6.1E-12
ADH1A[b]	Alcohol dehydrogenase 1A (class I), alpha polypeptide	1.42	−0.13	423.67	6.7E-12
KIAA1199	KIAA1199	0.66	1.82	423.25	6.7E-12
DDIT4	DNA-damage-inducible transcript 4	−1.52	−1.92	421.10	6.8E-12
AKR1C3[b]	Aldo-keto reductase family 1, member C3	1.72	1.22	416.81	7.2E-12
SFRP2	Secreted frizzled-related protein 2	1.84	0.48	414.62	7.3E-12
MMP13[a]	Matrix metallopeptidase 13 (collagenase 3)	−0.23	1.37	412.35	7.4E-12
MMP7[a]	Matrix metallopeptidase 7 (matrilysin, uterine)	−1.66	−0.57	400.33	9.1E-12
MRPS6[b]	Mitochondrial ribosomal protein S6	1.61	1.28	397.86	9.3E-12
PAPPA	Pregnancy-associated plasma protein A, pappalysin 1	1.61	0.43	396.32	9.4E-12
ALDOC[b]	Aldolase C, fructose-bisphosphate	−1.60	−1.44	395.05	9.4E-12
SLC1A3	Solute carrier family 1 (glial high affinity glutamate transporter), member 3	1.45	0.06	385.82	1.1E-11
CA12[b]	Carbonic anhydrase XII	−1.41	−1.41	375.18	1.3E-11
SEPX1	Selenoprotein X, 1	−1.09	0.49	371.63	1.4E-11
DIO2[b]	Deiodinase, iodothyronine, type II	1.56	1.61	368.77	1.4E-11
PFKFB4[b]	6-Phosphofructo-2-kinase/fructose-2,6-biphosphatase 4	−1.41	−1.36	367.05	1.4E-11
S100A8	S100 calcium binding protein A8	−1.57	−1.03	359.30	1.6E-11
INHBB	Inhibin, beta B	−1.46	−1.29	358.39	1.6E-11

Linear modeling was used to analyze differential expression. Log-fold changes are presented relative to untreated OS samples. Up-regulation is denoted by positive values, while down-regulation is denoted by negative values. Genes are ranked according to F-statistic. *p*-Values were adjusted as described in Materials and Methods section.

[a]Genes related to cell structure, adhesion, migration, and remodeling.

[b]Genes related to metabolism and mitochondria.

OS, untreated osteogenic; OB, ouabain-treated (10 nM); HK, high-K^+-treated (40 mM K^+).

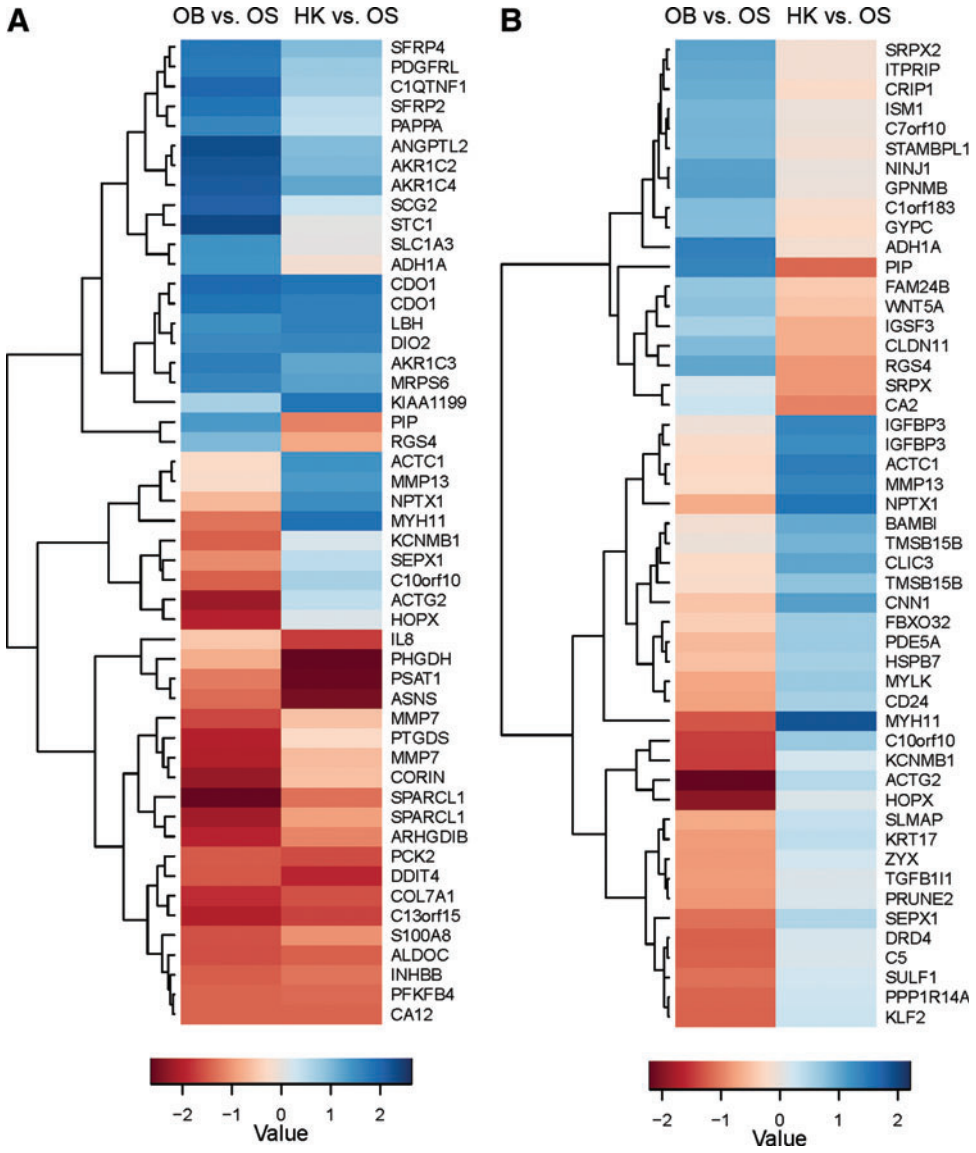

FIG. 5. Heatmaps of differentially expressed genes in OB- and HK-treated groups compared with the untreated OS group. **(A)** Log-fold differential gene expression in OB- and HK-treated groups compared with the OS group (left and right columns, respectively) is represented by a colormap (blue = up-regulated; red = down-regulated). See Table 2 for gene names associated with gene symbols. **(B)** Differentially expressed genes responding in opposite directions to OB- and HK-treatments. Log-fold differential expression is represented by a colormap (blue = up-regulated; red = down-regulated). See Table 3 for gene names associated with gene symbols. OB, ouabain-treated (10 nM); HK, high-K^+-treated (40 mM K^+). Color images available online at www.liebertpub.com/tea

point along the differentiation path, where they are committed to differentiate, as evidenced by the expression of some differentiated tissue markers, but they also possess more inter-lineage plasticity, allowing them to switch lineages more easily than nontreated cells. In this intermediate state, the cells increase their multi-lineage differentiation capacity, which is a property of their parent MSCs that persists late into the differentiation process,[90] but do not reacquire the stem-associated transcript profile, which may be a stem feature that is lost early in the differentiation process.

We profiled the transcriptional state of predifferentiated osteoblasts treated with OB and HK to identify potential mechanisms that mediate voltage signaling. Several cell cycle-related pathways were identified by GSEA analysis, which is consistent with previous reports that V_{mem} can regulate proliferation and cell cycle progression in various cell types.[23,24] Metabolism-related pathways were also identified by PCA, differential expression analysis, and GSEA. One potential mediator of metabolic-electric coupling is the ATP-sensitive K^+ channel (K_{ATP})[91–93]: K_{ATP} channel expression levels change on hMSC differentiation, and pharmacologic targeting of the channel can augment differentiation.[45,94] The cytoskeleton has also been identified by microarray analysis as a possible mediator of the depolarization response. This is supported by previous work demonstrating that V_{mem} depolarization and hyperpolarization affect actin and tubulin cytoskeleton organization[95–97] and that ion transport proteins and cytoskeletal proteins can interact directly to regulate each other's functions.[98–100] GSEA also implicated mRNA processing and protein degradation, both of which have been shown to be regulated by depolarization in neurons.[101–103]

Finally, a number of intracellular signaling pathways were also identified by differential gene expression analysis, including Rho, G-protein-coupled receptor (GPCR), inflammatory, and Wnt signaling. The Rho pathway has been shown to link transmembrane activity to cell adhesion and migration in neurons.[104] GPCRs can be activated by V_{mem} depolarization in muscle, and their voltage sensitivity may

Table 3. Top 50 Differentially Expressed Genes Responding in Opposite Directions in OB and HK Groups

Gene symbol	*Gene name*	*Log-fold change in OB*	*Log-fold change in HK*	*F-statistic*	*Adjusted p-value*
MYH11[a,b]	Myosin, heavy chain 11, smooth muscle	−1.29	1.87	1374.81	2.2E-14
ACTG2[a,b]	Actin, gamma 2, smooth muscle, enteric	−2.20	0.44	1080.05	6.7E-14
PIP	Prolactin-induced protein	1.36	−1.16	864.08	1.3E-13
HOPX	HOP homeobox	−1.96	0.15	772.65	2.4E-13
NPTX1	Neuronal pentraxin I	−0.67	1.53	722.30	3.3E-13
C10orf10	Chromosome 10 open reading frame 10	−1.44	0.66	663.03	4.5E-13
RGS4	Regulator of G-protein signaling 4	1.02	−0.83	493.43	2.8E-12
ACTC1[a,b]	Actin, alpha, cardiac muscle 1	−0.27	1.45	470.89	3.8E-12
KCNMB1	Potassium large conductance calcium-activated channel, subfamily M, beta member 1	−1.46	0.19	464.91	3.9E-12
ADH1A	Alcohol dehydrogenase 1A (class I), alpha polypeptide	1.42	−0.13	423.67	6.7E-12
MMP13[a]	Matrix metallopeptidase 13 (collagenase 3)	−0.23	1.37	412.35	7.4E-12
SEPX1	Selenoprotein X, 1	−1.09	0.49	371.63	1.4E-11
CNN1[a,b]	Calponin 1, basic, smooth muscle	−0.46	1.08	355.58	1.7E-11
KLF2	Kruppel-like factor 2 (lung)	−1.20	0.28	346.69	1.9E-11
DRD4	Dopamine receptor D4	−1.21	0.18	325.98	2.9E-11
CLDN11	Claudin 11	0.84	−0.64	314.05	3.7E-11
C5	Complement component 5	−1.19	0.16	308.65	4.0E-11
PPP1R14A[b]	Protein phosphatase 1, regulatory (inhibitor) subunit 14A	−1.18	0.27	306.52	4.1E-11
IGFBP3	Insulin-like growth factor binding protein 3	−0.07	1.34	275.64	8.2E-11
CLIC3	Chloride intracellular channel 3	−0.24	1.04	251.14	1.4E-10
SULF1	Sulfatase 1	−1.10	0.22	251.11	1.4E-10
MYLK[b]	Myosin light chain kinase	−0.71	0.65	248.22	1.5E-10
CA2	Carbonic anhydrase II	0.28	−0.97	247.55	1.5E-10
SRPX2[a]	Sushi-repeat-containing protein, X-linked 2	1.05	−0.11	234.70	2.1E-10
GPNMB[a]	Glycoprotein (transmembrane) nmb	1.09	−0.03	225.44	2.7E-10
CD24[a]	CD24 molecule	−0.74	0.56	222.69	2.8E-10
CRIP1	Cysteine-rich protein 1 (intestinal)	0.96	−0.21	217.71	3.2E-10
NINJ1[a]	Ninjurin 1	1.08	0.00	217.66	3.2E-10
IGFBP3	Insulin-like growth factor binding protein 3	−0.20	1.28	215.70	3.4E-10
ITPRIP	Inositol 1,4,5-triphosphate receptor interacting protein	0.99	−0.11	209.62	4.0E-10
IGSF3	Immunoglobulin superfamily, member 3	0.55	−0.65	204.25	4.5E-10
PDE5A[b]	Phosphodiesterase 5A, cGMP-specific	−0.55	0.64	201.32	5.0E-10
WNT5A	Wingless-type MMTV integration site family, member 5A	0.76	−0.46	198.23	5.5E-10
KRT17	Keratin 17	−0.80	0.38	190.14	7.0E-10
BAMBI	BMP and activin membrane-bound inhibitor homolog (Xenopuslaevis)	−0.10	0.98	190.04	7.0E-10
FAM24B	Family with sequence similarity 24, member B	0.71	−0.40	170.66	1.3E-09
SRPX[a]	Sushi-repeat-containing protein, X-linked	0.18	−0.83	166.68	1.5E-09
ZYX[a]	Zyxin	−0.81	0.22	164.81	1.7E-09
STAMBPL1	STAM binding protein-like 1	0.88	−0.10	164.44	1.7E-09
TMSB15B[a]	Thymosin beta 15B	−0.05	0.91	162.26	1.8E-09
C1orf183	Chromosome 1 open reading frame 183	0.81	−0.16	154.06	2.5E-09
PRUNE2	Prune homolog 2 (Drosophila)	−0.83	0.16	152.83	2.6E-09
HSPB7	Heat shock 27 kDa protein family, member 7 (cardiovascular)	−0.50	0.58	151.71	2.7E-09
C7orf10	Chromosome 7 open reading frame 10	0.90	−0.05	148.01	3.0E-09
FBXO32[b]	F-box protein 32	−0.38	0.63	147.78	3.0E-09
TGFB1I1	Transforming growth factor beta 1 induced transcript 1	−0.80	0.14	147.22	3.1E-09
GYPC	Glycophorin C (Gerbich blood group)	0.80	−0.24	147.01	3.1E-09
SLMAP	Sarcolemma associated protein	−0.68	0.34	145.37	3.3E-09
ISM1	Isthmin 1 homolog (zebrafish)	0.88	−0.03	143.06	3.7E-09
TMSB15B	Thymosin beta 15B	−0.19	0.75	141.87	3.8E-09

Linear modeling was used to analyze differential expression, and results were filtered for opposing responses in OB samples compared with HK samples. Log-fold changes are presented relative to untreated OS samples. Up-regulation is denoted by positive values, while down-regulation is denoted by negative values. Genes are ranked according to F-statistic. *p*-Values were adjusted as described in Materials and Methods section.

[a]Genes related to cell structure, adhesion, migration, and remodeling.

[b]Genes related to muscle cells and muscle functions.

OB, ouabain-treated (10 nM); HK, high-K^+-treated (40 mM K^+).

Table 4. Top 20 Pathways Identified by GSEA Analysis as Enriched in HK Or OB Groups

Comparison	*Pathway name*	*Pathway source*	*Size*	*NES*
HK vs. OS				
	Cell cycle regulation			
	CDT1 association with the CDC6 ORC origin complex	Reactome	52	1.98
	SCF SKP2-mediated degradation of p27 p21	Reactome	51	1.97
	Cyclin-E-associated events during G1 S transition	Reactome	57	1.96
	Autodegradation of CDH1 by CDH1 APC	Reactome	57	1.93
	M G1 transition	Reactome	61	1.93
	CDC20 phospho APC-mediated degradation of cyclin A	Reactome	62	1.92
	Protein degradation and proteasome function			
	VIF-mediated degradation of APOBEC3G	Reactome	47	1.97
	SCF-SKP2-mediated degradation of p27 p21	Reactome	51	1.97
	Proteasome	KEGG	44	1.94
	Autodegradation of CDH1 by CDH1 APC	Reactome	57	1.93
	CDC20 phospho APC-mediated degradation of cyclin A	Reactome	62	1.92
	Regulation of ornithine decarboxylase	Reactome	46	1.92
	mRNA processing			
	mRNA splicing minor pathway	Reactome	39	1.96
	Spliceosome	KEGG	118	1.93
	Elongation and processing of capped transcripts	Reactome	123	1.93
	mRNA splicing	Reactome	96	1.91
	Formation and maturation of mRNA transcript	Reactome	141	1.90
	Metabolism			
	Citric acid cycle	Reactome	19	1.93
	Electron transport chain	Reactome	59	1.91
	Other			
	Stabilization of p53	Reactome	46	1.95
	p53 Independent DNA damage response	Reactome	43	1.94
	Membrane trafficking	Reactome	77	1.94
	Signaling by Wnt	Reactome	57	1.91
OB vs. OS				
	Cell cycle regulation			
	CDT1 association with the CDC6 ORC origin complex	Reactome	52	2.04
	SCF SKP2-mediated degradation of p27 p21	Reactome	51	2.03
	Autodegradation of CDH1 by CDH1 APC	Reactome	57	2.02
	M G1 transition	Reactome	61	2.02
	SCF beta TRCP-mediated degradation of EMI1	Reactome	47	2.01
	Protein degradation and proteasome function			
	VIF-mediated degradation of APOBEC3G	Reactome	47	2.10
	Regulation of ornithine decarboxylase	Reactome	46	2.03
	SCF SKP2-mediated degradation of p27 p21	Reactome	51	2.03
	Autodegradation of CDH1 by CDH1 APC	Reactome	57	2.02
	SCF beta TRCP-mediated degradation of EMI1	Reactome	47	2.01
	mRNA Transcription and translation			
	Influenza viral RNA transcription and replication	Reactome	97	2.02
	Peptide chain elongation	Reactome	83	2.02
	Ribosome	KEGG	85	2.02
	Viral mRNA translation	Reactome	83	2.02
	Metabolism			
	Electron transport chain	Reactome	59	2.18
	Oxidative phosphorylation	KEGG	110	2.13
	Citric acid cycle	Reactome	19	2.10
	Pyruvate metabolism and TCA cycle	Reactome	35	2.03
	Insulin-related Pathways			
	Glucose regulation of insulin secretion	Reactome	141	2.06
	Insulin synthesis and secretion	Reactome	127	2.02
	Other			
	Parkinson's disease	KEGG	105	2.06
	Signaling by Wnt	Reactome	57	2.04
	p53 Independent DNA damage response	Reactome	43	2.02

Pathway enrichment was analyzed using the curated canonical pathways (CP) gene sets from Molecular Signatures Database. The source of each pathway is indicated. Size indicates the number of genes comprising the pathway. Pathways are ranked according to Normalized Enrichment Score (NES) within each category.

HK, high-K^+-treated (40 mM K^+); GSEA, gene set enrichment analysis; KEGG, kyoto encyclopedia of genes and genomes.

Table 5. Top 10 Pathways Identified by GSEA Analysis as Enriched in HK Versus OB

Pathway name	*Pathway source*	*Size*	*NES*
Muscle function			
Muscle contraction	Reactome	50	−2.63
Smooth muscle contraction	Reactome	23	−2.36
Vascular smooth muscle contraction	KEGG	112	−2.05
Semaphorin and Rho signaling			
Rho pathway	Biocarta	32	−2.09
Sema4D-induced cell migration and growth cone collapse	Reactome	23	−2.05
Sema4D in semaphorin signaling	Reactome	28	−2.04
Semaphorin interactions	Reactome	64	−1.98
Extracellular matrix and integrin interactions			
Cell extracellular matrix interactions	Reactome	16	−2.02
Integrin cell surface interactions	Reactome	81	−1.93
Other			
Steroid biosynthesis	KEGG	17	−1.91

Pathway enrichment was analyzed using the curated canonical pathways (CP) gene sets from Molecular Signatures Database. The source of each pathway is indicated. Size indicates the number of genes comprising the pathway. Pathways are ranked according to Normalized Enrichment Score (NES) within each category.

OB, ouabain-treated (10 nM); HK, high-K^+-treated (40 mM K^+).

be due to voltage-dependent charge movements.[105,106] Inflammatory cytokines can be modulated by and can also induce depolarization.[107–109] The Wnt pathway, a critical regulator of many osteoblast functions, including bone differentiation, maturation, homeostasis, and repair, has been shown to be required for establishing an electrical gradient across the developing heart.[110–112]

The present study has shown that voltage modulation in osteoblasts and adipocytes can induce changes in cell phenotype, which is reminiscent of dedifferentiation events seen

Table 6. Leading Edge Genes for GSEA Enrichment Results: Top 50 Genes for HK Versus OS and Top 50 Genes for OB Versus OS

HK vs. OS		*OB vs. OS*	
Symbol	*Gene name*	*Symbol*	*Gene name*
PSMD 1–8,10,12–14	Proteasome 26S subunit, non-ATPase, 1–8, 10, 12–14	*UBB*	Ubiquitin B
PSMA 1–6	Proteasome subunit, alpha type, 1–6	*PSMD 1–10,12–14*	Proteasome 26S subunit, non-ATPase, 1–10, 12–14
PSMB 1–6,8,10	Proteasome subunit, beta type, 1–6, 8, 10	*PSMA 1–6*	Proteasome subunit, alpha type, 1–6
PSMC 1–6	Proteasome 26S subunit, ATPase, 1–6	*PSMB 1–8,10*	Proteasome subunit, beta type, 1–8, 10
PSME 1–3	Proteasome activator subunit 1 (PA28 alpha)	*PSMC 1–6*	Proteasome 26S subunit, ATPase, 1–6
PSMF1	Proteasome inhibitor subunit 1 (PI31)	*PSME 1–3*	Proteasome activator subunit 1 (PA28 alpha)
UBB	Ubiquitin B	*SDH A,B,C,D*	Succinate dehydrogenase complex, subunits A, B, C, D
SFRS 1,2,6,7	Splicing factor, arginine/serine-rich 1, 2, 6, 7	*RPL 13,14,17,18*	Ribosomal protein L13, 14, 17, 18
LSM2	LSM2 homolog, U6 small nuclear RNA associated (S. cerevisiae)	*RPLP 0, 1, 2*	Ribosomal protein, large, P0, 1, 2
SF3B14	Splicing factor 3B, 14 kDa subunit		
SFRS 1, 2	Splicing factor, arginine/serine-rich 1, 2 (splicing factor 2, alternate splicing factor)		
NHP2L1	NHP2 nonhistone chromosome protein 2-like 1 (S. cerevisiae)		
SF3B 1–5	Splicing factor 3b, subunits 1–5		
TXNL4A	Thioredoxin-like 4A		

Leading edge genes from top HK- and OB-enriched pathways (Table 4) are ranked according to their frequency of appearance in the enriched pathways. Leading edge genes are those that contribute most to a pathway's enrichment score.

OB, ouabain-treated (10 nM); HK, high-K^+-treated (40 mM K^+).

Table 7. Leading Edge Genes for GSEA Enrichment Results: Top 20 Genes for HK Versus OB

HK vs. OB	
Symbol	*Gene name*
MYL9	Myosin, light chain 9, regulatory
MYH11	Myosin, heavy chain 11, smooth muscle
ITGA1	Integrin, alpha 1
MYLK	Myosin, light chain kinase
ROCK2	Rho-associated, coiled-coil containing protein kinase 2
RHOA	Ras homolog gene family, member A
LIMK1	LIM domain kinase 1
VCL	Vinculin
ACTG2	Actin, gamma 2, smooth muscle, enteric
TLN1	Talin 1
PLXNB1	Plexin B1
MYH9	Myosin, heavy chain 9, nonmuscle
ERBB2	V-erb-b2 erythroblastic leukemia viral oncogene homolog 2
RAC2	Ras-related C3 botulinum toxin substrate 2
CDC42	Cell division cycle 42 (GTP binding protein, 25 kDa)
RHOB	Ras homolog gene family, member B
PPP1R12B	Protein phosphatase 1, regulatory (inhibitor) subunit 12B
MYL2	Myosin, light chain 2, regulatory, cardiac, slow
LMOD1	Leiomodin 1 (smooth muscle)
TPM1	Tropomyosin 1 (alpha)

Leading edge genes from top enriched pathways in HK versus OB (Table 5) are ranked according to their frequency of appearance in the enriched pathways. Leading edge genes are those that contribute most to a pathway's enrichment score.

OB, ouabain-treated (10 nM); HK, high-K^+-treated (40 mM K^+).

in wound healing *in vivo*. Depolarized cells do not completely revert back to the stem state, but in the case of osteoblasts, they retain their multipotentiality. Several mechanisms have been identified by microarray analysis, but further studies are necessary to determine whether these pathways, indeed, functionally participate in transducing voltage signals into cellular behaviors. Also of interest is whether the depolarization response recruits similar pathways as *in vivo* dedifferentiation events during regeneration.[15] Data mining using publicly available microarray data from wound healing and regeneration experiments may facilitate such a comparative analysis.

Future studies may employ *in vitro* and *in vivo* wound healing models to explore how bioelectric events may direct regeneration-related cell functions in the context of the wound environment. It will be interesting to test whether bioelectric signaling can trigger events that recapitulate other aspects of *in vivo* regeneration, such as formation of a blastema at the injury site, or establishment of correct tissue patterning. A better understanding of how bioelectric signaling affects the healing process would be a step forward in developing alternative tissue regeneration strategies that complement current adult stem cell transplantation approaches.

Acknowledgments

The authors thank the Tufts Center for Neuroscience Research (P30 NS047243) and the Yale Center for Genome Analysis for assistance with microarray experiments. S.S. thanks the NSF for funding through the Graduate Research Fellowship Program. The authors also thank the NIH for support through the Tissue Engineering Resource Center (P41 EB002520), R01 AR005593, and R01 AR061988.

Disclosure Statement

No competing financial interests exist.

References

1. Abdallah, B.M., and Kassem, M. Human mesenchymal stem cells: from basic biology to clinical applications. Gene Ther **15,** 109, 2008.
2. Barry, F.P., and Murphy, J.M. Mesenchymal stem cells: clinical applications and biological characterization. Int J Biochem Cell Biol **36,** 568, 2004.
3. Orlic, D., Hill, J.M., and Arai, A.E. Stem cells for myocardial regeneration. Circ Res **91,** 1092, 2002.
4. Salem, H.K., and Thiemermann, C. Mesenchymal stromal cells: current understanding and clinical status. Stem Cells **28,** 585, 2010.
5. Pittenger, M.F., Mackay, A.M., Beck, S.C., Jaiswal, R.K., Douglas, R., Mosca, J.D., Moorman, M.A., Simonetti, D.W., Craig, S., and Marshak, D.R. Multilineage potential of adult human mesenchymal stem cells. Science **284,** 143, 1999.
6. Bonab, M.M., Alimoghaddam, K., Talebian, F., Ghaffari, S.H., Ghavamzadeh, A., and Nikbin, B. Aging of mesenchymal stem cell *in vitro*. BMC Cell Biol **7,** 14, 2006.
7. Wagner, W., Horn, P., Castoldi, M., Diehlmann, A., Bork, S., Saffrich, R., Benes, V., Blake, J., Pfister, S., Eckstein, V., and Ho, A.D. Replicative senescence of mesenchymal stem cells: a continuous and organized process. PLoS One **3,** e2213, 2008.
8. Bentzon, J.F., Stenderup, K., Hansen, F.D., Schroder, H.D., Abdallah, B.M., Jensen, T.G., and Kassem, M. Tissue distribution and engraftment of human mesenchymal stem cells immortalized by human telomerase reverse transcriptase gene. Biochem Biophys Res Commun **330,** 633, 2005.
9. François, S., Bensidhoum, M., Mouiseddine, M., Mazurier, C., Allenet, B., Semont, A., Frick, J., Saché, A., Bouchet, S., Thierry, D., Gourmelon, P., Gorin, N.C., and Chapel, A. Local irradiation not only induces homing of human mesenchymal stem cells at exposed sites but promotes their widespread engraftment to multiple organs: a study of their quantitative distribution after irradiation damage. Stem Cells **24,** 1020, 2006.
10. Gao, J., Dennis, J.E., Muzic, R.F., Lundberg, M., and Caplan, A.I. The dynamic *in vivo* distribution of bone marrow-derived mesenchymal stem cells after infusion. Cells Tissues Organs **169,** 12, 2001.
11. Chen, Z.L., Yu, W.M., and Strickland, S. Peripheral regeneration. Annu Rev Neurosci **30,** 209, 2007.
12. Jopling, C., Boue, S., and Izpisua Belmonte, J.C. Dedifferentiation, transdifferentiation and reprogramming: three routes to regeneration. Nat Rev Mol Cell Biol **12,** 79, 2011.
13. Jopling, C., Sleep, E., Raya, M., Marti, M., Raya, A., and Izpisua Belmonte, J.C. Zebrafish heart regeneration occurs by cardiomyocyte dedifferentiation and proliferation. Nature **464,** 606, 2010.
14. Kikuchi, K., Holdway, J.E., Werdich, A.A., Anderson, R.M., Fang, Y., Egnaczyk, G.F., Evans, T., Macrae, C.A., Stainier, D.Y., and Poss, K.D. Primary contribution to zebrafish

heart regeneration by gata4(+) cardiomyocytes. Nature **464,** 601, 2010.
15. Knopf, F., Hammond, C., Chekuru, A., Kurth, T., Hans, S., Weber, C.W., Mahatma, G., Fisher, S., Brand, M., Schulte-Merker, S., and Weidinger, G. Bone regenerates via dedifferentiation of osteoblasts in the zebrafish fin. Dev Cell **20,** 713, 2011.
16. Kragl, M., Knapp, D., Nacu, E., Khattak, S., Maden, M., Epperlein, H.H., and Tanaka, E.M. Cells keep a memory of their tissue origin during axolotl limb regeneration. Nature **460,** 60, 2009.
17. Mirsky, R., Woodhoo, A., Parkinson, D.B., Arthur-Farraj, P., Bhaskaran, A., and Jessen, K.R. Novel signals controlling embryonic Schwann cell development, myelination and dedifferentiation. J Peripher Nerv Syst **13,** 122, 2008.
18. Tanaka, E.M., Gann, A.A., Gates, P.B., and Brockes, J.P. Newt myotubes reenter the cell cycle by phosphorylation of the retinoblastoma protein. J Cell Biol **136,** 155, 1997.
19. Song, L., Webb, N.E., Song, Y., and Tuan, R.S. Identification and functional analysis of candidate genes regulating mesenchymal stem cell self-renewal and multipotency. Stem Cells **24,** 1707, 2006.
20. Liu, Y., Jiang, X., Zhang, X., Chen, R., Sun, T., Fok, K.L., Dong, J., Tsang, L.L., Yi, S., Ruan, Y., Guo, J., Yu, M.K., Tian, Y., Chung, Y.W., Yang, M., Xu, W., Chung, C.M., Li, T., and Chan, H.C. Dedifferentiation-reprogrammed mesenchymal stem cells with improved therapeutic potential. Stem Cells **29,** 2077, 2011.
21. Levin, M. Bioelectric mechanisms in regeneration: unique aspects and future perspectives. Semin Cell Dev Biol **20,** 543, 2009.
22. Levin, M. Endogenous bioelectric signals as morphogenetic controls of development, regeneration, and neoplasm. In: Pullar, C.E., ed. The Physiology of Bioelectricity in Development, Tissue Regeneration, and Cancer. Boca Raton, FL: CRC Press, 2011, pp. 39–89.
23. Blackiston, D.J., McLaughlin, K.A., and Levin, M. Bioelectric controls of cell proliferation: ion channels, membrane voltage and the cell cycle. Cell Cycle **8,** 3527, 2009.
24. Sundelacruz, S., Levin, M., and Kaplan, D.L. Role of membrane potential in the regulation of cell proliferation and differentiation. Stem Cell Rev Rep **5,** 231, 2009.
25. Levin, M. Large-scale biophysics: ion flows and regeneration. Trends Cell Biol **17,** 261, 2007.
26. Levin, M. Molecular bioelectricity in developmental biology: new tools and recent discoveries: control of cell behavior and pattern formation by transmembrane potential gradients. Bioessays **34,** 205, 2012.
27. Adams, D.S., Masi, A., and Levin, M. H+ pump-dependent changes in membrane voltage are an early mechanism necessary and sufficient to induce Xenopus tail regeneration. Development **134,** 1323, 2007.
28. Altizer, A.M., Stewart, S.G., Albertson, B.K., and Borgens, R.B. Skin flaps inhibit both the current of injury at the amputation surface and regeneration of that limb in newts. J Exp Zool **293,** 467, 2002.
29. Beane, W.S., Morokuma, J., Adams, D.S., and Levin, M. A chemical genetics approach reveals H,K-ATPase-mediated membrane voltage is required for planarian head regeneration. Chem Biol **18,** 77, 2011.
30. Jenkins, L.S., Duerstock, B.S., and Borgens, R.B. Reduction of the current of injury leaving the amputation inhibits limb regeneration in the red spotted newt. Dev Biol **178,** 251, 1996.
31. Tseng, A.S., Beane, W.S., Lemire, J.M., Masi, A., and Levin, M. Induction of vertebrate regeneration by a transient sodium current. J Neurosci **30,** 13192, 2010.
32. Pai, V.P., Aw, S., Shomrat, T., Lemire, J.M., and Levin, M. Transmembrane voltage potential conrols embryonic eye patterning in Xenopus laevis. Development **139,** 313, 2012.
33. Vandenberg, L.N., Morrie, R.D., and Adams, D.S. V-ATPase-dependent ectodermal voltage and pH regionalization are required for craniofacial morphogenesis. Dev Dyn **240,** 1889, 2011.
34. Konig, S., Hinard, V., Arnaudeau, S., Holzer, N., Potter, G., Bader, C.R., and Bernheim, L. Membrane hyperpolarization triggers myogenin and myocyte enhancer factor-2 expression during human myoblast differentiation. J Biol Chem **279,** 28187, 2004.
35. Liu, J.H., Bijlenga, P., Fischer-Lougheed, J., Occhiodoro, T., Kaelin, A., Bader, C.R., and Bernheim, L. Role of an inward rectifier K+ current and of hyperpolarization in human myoblast fusion. J Physiol **510,** 467, 1998.
36. Fischer-Lougheed, J., Liu, J.H., Espinos, E., Mordasini, D., Bader, C.R., Belin, D., and Bernheim, L. Human myoblast fusion requires expression of functional inward rectifier Kir2.1 channels. J Cell Biol **153,** 677, 2001.
37. Hinard, V., Belin, D., Konig, S., Bader, C.R., and Bernheim, L. Initiation of human myoblast differentiation via dephosphorylation of Kir2.1 K+ channels at tyrosine 242. Development **135,** 859, 2008.
38. Konig, S., Béguet, A., Bader, C.R., and Bernheim, L. The calcineurin pathway links hyperpolarization (Kir2.1)-induced Ca2+ signals to human myoblast differentiation and fusion. Development **133,** 3107, 2006.
39. van Vliet, P., de Boer, T.P., van der Heyden, M.A.G., Tamer, M.K.E., Sluijter, J.P.G., Doevendans, P.A., and Goumans, M.J. Hyperpolarization induces differentiation in human cardiomyocyte progenitor cells. Stem Cell Rev Rep **6,** 178, 2010.
40. Arcangeli, A., Bianchi, L., Becchetti, A., Faravelli, L., Coronnello, M., Mini, E., Olivotto, M., and Wanke, E. A novel inward-rectifying K+ current with a cell-cycle dependence governs the resting potential of mammalian neuroblastoma cells. J Physiol **489,** 455, 1995.
41. Arcangeli, A., Rosati, B., Cherubini, A., Crociani, O., Fontana, L., Passani, B., Wanke, E., and Olivotto, M. Long term exposure to retinoic acid induces the expression of IRK1 channels in HERG channel-endowed neuroblastoma cells. Biochem Biophys Res Commun **244,** 706, 1998.
42. Arcangeli, A., Rosati, B., Cherubini, A., Crociani, O., Fontana, L., Ziller, C., Wanke, E., and Olivotto, M. HERG- and IRK-like inward rectifier currents are sequentially expressed during neuronal development of neural crest cells and their derivatives. Eur J Neurosci **9,** 2596, 1997.
43. Arcangeli, A., Rosati, B., Crociani, O., Cherubini, A., Fontana, L., Passani, B., Wanke, E., and Olivotto, M. Modulation of HERG current and herg gene expression during retinoic acid treatment of human neuroblastoma cells: potentiating effects of BDNF. J Neurobiol **40,** 214, 1999.
44. Ng, S.Y., Chin, C.H., Lau, Y.T., Luo, J., Wong, C.K., Bian, Z.X., and Tsang, S.Y. Role of voltage-gated potassium channels in the fate determination of embryonic stem cells. J Cell Physiol **224,** 165, 2010.
45. Sundelacruz, S., Levin, M., and Kaplan, D.L. Membrane potential controls adipogenic and osteogenic differentiation of mesenchymal stem cells. PLoS One **3,** e3737, 2008.

46. Schilling, T., Kuffner, R., Klein-Hitpass, L., Zimmer, R., Jakob, F., and Schutze, N. Microarray analyses of transdifferentiated mesenchymal stem cells. J Cell Biochem **103,** 413, 2008.
47. Schilling, T., Noth, U., Klein-Hitpass, L., Jakob, F., and Schutze, N. Plasticity in adipogenesis and osteogenesis of human mesenchymal stem cells. Mol Cell Endocrinol **271,** 1, 2007.
48. Liu, F., Akiyama, Y., Tai, S., Maruyama, K., Kawaguchi, Y., Muramatsu, K., and Yamaguchi, K. Changes in the expression of CD106, osteogenic genes, and transcription factors involved in the osteogenic differentiation of human bone marrow mesenchymal stem cells. J Bone Miner Metab **26,** 312, 2008.
49. Collard, J.F., Mertens, B., and Hinsenkamp, M. *In vitro* study of the effects of ELF electric fields on gene expression in human epidermal cells. Bioelectromagnetics **32,** 28, 2011.
50. Hinsenkamp, M., and Collard, J.F. Bone Morphogenic Protein - MRNA upregulation after exposure to low frequency electric field. Int Orthop **35,** 1577, 2011.
51. Martherus, R.S.R.M., Vanherle, S.J.V., Timmer, E.D.J., Zeijlemaker, V.A., Broers, J.L., Smeets, H.J., Geraedts, J.P., and Ayoubi, T.A.Y. Electrical signals affect the cardiomyocyte transcriptome independently of contraction. Physiol Genomics **42A,** 283, 2010.
52. Sollazzo, V., Palmieri, A., Pezzetti, F., Massari, L., and Carinci, F. Effects of pulsed electromagnetic fields on human osteoblastlike cells (MG-63): a pilot study. Clin Orthop Relat Res **468,** 2260, 2010.
53. Mauney, J.R., Nguyen, T., Gillen, K., Kirker-Head, C., Gimble, J.M., and Kaplan, D.L. Engineering adipose-like tissue *in vitro* and *in vivo* utilizing human bone marrow and adipose-derived mesenchymal stem cells with silk fibroin 3D scaffolds. Biomaterials **28,** 5280, 2007.
54. Meinel, L., Fajardo, R., Hofmann, S., Langer, R., Chen, J., Snyder, B., Vunjak-Novakovic, G., and Kaplan, D. Silk implants for the healing of critical size bone defects. Bone **37,** 688, 2005.
55. Meinel, L., Hofmann, S., Betz, O., Fajardo, R., Merkle, H.P., Langer, R., Evans, C.H., Vunjak-Novakovic, G., and Kaplan, D.L. Osteogenesis by human mesenchymal stem cells cultured on silk biomaterials: comparison of adenovirus mediated gene transfer and protein delivery of BMP-2. Biomaterials **27,** 4993, 2006.
56. Du, P., Kibbe, W.A., and Lin, S.M. lumi: a pipeline for processing Illumina microarray. Bioinformatics **24,** 1547, 2008.
57. Lin, S.M., Du, P., Huber, W., and Kibbe, W.A. Model-based variance-stabilizing transformation for Illumina microarray data. Nucleic Acids Res **36,** e11, 2008.
58. Smyth, G.K. Linear models and empirical bayes methods for assessing differential expression in microarray experiments. Stat Appl Genet Mol Biol **3,** Article 3, 2004.
59. Gentleman, R. Using GO for statistical analyses. COMPSTAT 2004—Proceedings in Computational Statistics: 16th Symposium Held in Prague, Czech Republic, 171, 2004.
60. Supek, F., Bosnjak, M., Skunca, N., and Smuc, T. Revigo summarizes and visualizes long lists of gene ontology terms. PLoS One **6,** e21800, 2011.
61. Mootha, V.K., Lindgren, C.M., Eriksson, K.F., Subramanian, A., Sihag, S., Lehar, J., Puigserver, P., Carlsson, E., RidderstrÃ¥le, M., Laurila, E., Houstis, N., Daly, M.J., Patterson, N., Mesirov, J.P., Golub, T.R., Tamayo, P., Spiegelman, B., Lander, E.S., Hirschhorn, J.N., Altshuler, D., and Groop, L.C. PGC-1alpha-responsive genes involved in oxidative phosphorylation are coordinately downregulated in human diabetes. Nat Genet **34,** 267, 2003.
62. Subramanian, A., Tamayo, P., Mootha, V.K., Mukherjee, S., Ebert, B.L., Gillette, M.A., Paulovich, A., Pomeroy, S.L., Golub, T.R., Lander, E.S., and Mesirov, J.P. Gene set enrichment analysis: a knowledge-based approach for interpreting genome-wide expression profiles. Proc Natl Acad Sci U S A **102,** 15545, 2005.
63. Song, L., and Tuan, R.S. Transdifferentiation potential of human mesenchymal stem cells derived from bone marrow. FASEB J **18,** 980, 2004.
64. Phinney, D.G., Kopen, G., Righter, W., Webster, S., Tremain, N., and Prockop, D.J. Donor variation in the growth properties and osteogenic potential of human marrow stromal cells. J Cell Biochem **75,** 424, 1999.
65. Siddappa, R., Licht, R., van Blitterswijk, C., and de Boer, J. Donor variation and loss of multipotency during *in vitro* expansion of human mesenchymal stem cells for bone tissue engineering. J Orthop Res **25,** 1029, 2007.
66. Akune, T., Ohba, S., Kamekura, S., Yamaguchi, M., Chung, U.I., Kubota, N., Terauchi, Y., Harada, Y., Azuma, Y., Nakamura, K., Kadowaki, T., and Kawaguchi, H. PPARγ insufficiency enhances osteogenesis through osteoblast formation from bone marrow progenitors. J Clin Invest **113,** 846, 2004.
67. Beresford, J.N., Bennett, J.H., Devlin, C., Leboy, P.S., and Owen, M.E. Evidence for an inverse relationship between the differentiation of adipocytic and osteogenic cells in rat marrow stromal cell cultures. J Cell Sci **102,** 341, 1992.
68. Burkhardt, R., Kettner, G., Böhm, W., Schmidmeier, M., Schlag, R., Frisch, B., Mallmann, B., Eisenmenger, W., and Gilg, T. Changes in trabecular bone, hematopoiesis and bone marrow vessels in aplastic anemia, primary osteoporosis, and old age: a comparative histomorphometric study. Bone **8,** 157, 1987.
69. Jaiswal, R.K., Jaiswal, N., Bruder, S.P., Mbalaviele, G., Marshak, D.R., and Pittenger, M.F. Adult human mesenchymal stem cell differentiation to the osteogenic or adipogenic lineage is regulated by mitogen-activated protein kinase. J Biol Chem **275,** 9645, 2000.
70. Lecka-Czernik, B., Gubrij, I., Moerman, E.J., Kajkenova, O., Lipschitz, D.A., Manolagas, S.C., and Jilka, R.L. Inhibition of Osf2/Cbfa1 expression and terminal osteoblast differentiation by PPARγ2. J Cell Biochem **74,** 357, 1999.
71. Lecka-Czernik, B., Moerman, E.J., Grant, D.F., Lehmann, J.M., Manolagas, S.C., and Jilka, R.L. Divergent effects of selective peroxisome proliferator-activated receptor-γ2 ligands on adipocyte versus osteoblast differentiation. Endocrinology **143,** 2376, 2002.
72. Krishnan, V., Bryant, H.U., and MacDougald, O.A. Regulation of bone mass by Wnt signaling. J Clin Invest **116,** 1202, 2006.
73. Takada, I., Mihara, M., Suzawa, M., Ohtake, F., Kobayashi, S., Igarashi, M., Youn, M.Y., Takeyama, K.I., Nakamura, T., Mezaki, Y., Takezawa, S., Yogiashi, Y., Kitagawa, H., Yamada, G., Takada, S., Minami, Y., Shibuya, H., Matsumoto, K., and Kato, S. A histone lysine methyltransferase activated by non-canonical Wnt signalling suppresses PPAR-γ transactivation. Nat Cell Biol **9,** 1273, 2007.
74. Bowers, R.R., Kim, J.W., Otto, T.C., and Lane, M.D. Stable stem cell commitment to the adipocyte lineage by inhibition of DNA methylation: role of the BMP-4 gene. Proc Natl Acad Sci U S A **103,** 13022, 2006.

75. Bowers, R.R., and Lane, M.D. A role for bone morphogenetic protein-4 in adipocyte development. Cell Cycle **6,** 385, 2007.
76. Chen, D., Ji, X., Harris, M.A., Feng, J.Q., Karsenty, G., Celeste, A.J., Rosen, V., Mundy, G.R., and Harris, S.E. Differential roles for bone morphogenetic protein (BMP) receptor type IB and IA in differentiation and specification of mesenchymal precursor cells to osteoblast and adipocyte lineages. J Cell Biol **142,** 295, 1998.
77. Cheng, H., Jiang, W., Phillips, F.M., Haydon, R.C., Peng, Y., Zhou, L., Luu, H.H., An, N., Breyer, B., Vanichakarn, P., Szatkowski, J.P., Park, J.Y., and He, T.C. Osteogenic activity of the fourteen types of human bone morphogenetic proteins (BMPs). J Bone Joint Surg Series **A85,** 1544, 2003.
78. Kang, Q., and He, T.C. A comprehensive analysis of the dual roles of BMPs in regulating adipogenic and osteogenic differentiation of mesenchymal progenitor cells. Stem Cells Dev **18,** 545, 2008.
79. Suzawa, M., Takeuchi, Y., Fukumoto, S., Kato, S., Ueno, N., Miyazono, K., Matsumoto, T., and Fujita, T. Extracellular matrix-associated bone morphogenetic proteins are essential for differentiation of murine osteoblastic cells *in vitro*. Endocrinology **140,** 2125, 1999.
80. Hanada, K., Dennis, J.E., and Caplan, A.I. Stimulatory effects of basic fibroblast growth factor and bone morphogenetic protein-2 on osteogenic differentiation of rat bone marrow- derived mesenchymal stem cells. J Bone Miner Res **12,** 1606, 1997.
81. Neubauer, M., Fischbach, C., Bauer-Kreisel, P., Lieb, E., Hacker, M., Tessmar, J., Schulz, M.B., Goepferich, A., and Blunk, T. Basic fibroblast growth factor enhances PPARγ ligand-induced adipogenesis of mesenchymal stem cells. FEBS Lett **577,** 277, 2004.
82. Neubauer, M., Hacker, M., Bauer-Kreisel, P., Weiser, B., Fischbach, C., Schulz, M.B., Goepferich, A., and Blunk, T. Adipose tissue engineering based on mesenchymal stem cells and basic fibroblast growth factor *in vitro*. Tissue Eng **11,** 1840, 2005.
83. Pitaru, S., Kotev-Emeth, S., Noff, D., Kaffuler, S., and Savion, N. Effect of basic fibroblast growth factor on the growth and differentiation of adult stromal bone marrow cells: enhanced development of mineralized bone- like tissue in culture. J Bone Miner Res **8,** 919, 1993.
84. Koch, H., Jadlowiec, J.A., and Campbell, P.G. Insulin-like growth factor-I induces early osteoblast gene expression in human mesenchymal stem cells. Stem Cells Dev **14,** 621, 2005.
85. Scavo, L.M., Karas, M., Murray, M., and Leroith, D. Insulin-like growth factor-I stimulates both cell growth and lipogenesis during differentiation of human mesenchymal stem cells into adipocytes. J Clin Endocrinol Metab **89,** 3543, 2004.
86. Thomas, T., Gori, F., Spelsberg, T.C., Khosla, S., Riggs, B.L., and Conover, C.A. Response of bipotential human marrow stromal cells to insulin-like growth factors: effect on binding protein production, proliferation, and commitment to osteoblasts and adipocytes. Endocrinology **140,** 5036, 1999.
87. Celil, A.B., and Campbell, P.G. BMP-2 and insulin-like growth factor-I mediate osterix (Osx) expression in human mesenchymal stem cells via the MAPK and protein kinase D signaling pathways. J Biol Chem **280,** 31353, 2005.
88. Hata, K., Nishimura, R., Ikeda, F., Yamashita, K., Matsubara, T., Nokubi, T., and Yoneda, T. Differential roles of Smad1 and p38 kinase in regulation of peroxisome proliferator-activating receptor γ during bone morphogenetic protein 2-induced adipogenesis. Mol Biol Cell **14,** 545, 2003.
89. Hullinger, T.G., Pan, Q., Viswanathan, H.L., and Somerman, M.J. TGFβ and BMP-2 activation of the OPN promoter: roles of Smad- and Hox-binding elements. Exp Cell Res **262,** 69, 2001.
90. Ponce, M.L., Koelling, S., Kluever, A., Heinemann, D.E.H., Miosge, N., Wulf, G., Frosch, K.H., Schütze, N., Hufner, M., and Siggelkow, H. Coexpression of osteogenic and adipogenic differentiation markers in selected subpopulations of primary human mesenchymal progenitor cells. J Cell Biochem **104,** 1342, 2008.
91. Miki, T., and Seino, S. Roles of KATP channels as metabolic sensors in acute metabolic changes. J Mol Cell Cardiol **38,** 917, 2005.
92. Nichols, C.G. KATP channels as molecular sensors of cellular metabolism. Nature **440,** 470, 2006.
93. Zingman, L.V., Alekseev, A.E., Hodgson-Zingman, D.M., and Terzic, A. ATP-sensitive potassium channels: metabolic sensing and cardioprotection. J Appl Physiol **103,** 1888, 2007.
94. Diehlmann, A., Bork, S., Saffrich, R., Veh, R.W., Wagner, W., and Derst, C. KATP channels in mesenchymal stromal stem cells: strong up-regulation of Kir6.2 subunits upon osteogenic differentiation. Tissue Cell **43,** 331, 2011.
95. Chifflet, S., Hernandez, J.A., and Grasso, S. A possible role for membrane depolarization in epithelial wound healing. Am J Physiol Cell Physiol **288,** C1420, 2005.
96. Chifflet, S., Hernandez, J.A., Grasso, S., and Cirillo, A. Nonspecific depolarization of the plasma membrane potential induces cytoskeletal modifications of bovine corneal endothelial cells in culture. Exp Cell Res **282,** 1, 2003.
97. Nin, V., Hernandez, J.A., and Chifflet, S. Hyperpolarization of the plasma membrane potential provokes reorganization of the actin cytoskeleton and increases the stability of adherens junctions in bovine corneal endothelial cells in culture. Cell Motil Cytoskeleton **66,** 1087, 2009.
98. Arcangeli, A., and Becchetti, A. Complex functional interaction between integrin receptors and ion channels. Trends Cell Biol **16,** 631, 2006.
99. Chifflet, S., and Hernandez, J.A. The plasma membrane potential and the organization of the actin cytoskeleton of epithelial cells. Int J Cell Biol **2012,** 121424, 2012.
100. Davis, M.J., Wu, X., Nurkiewicz, T.R., Kawasaki, J., Gui, P., Hill, M.A., and Wilson, E. Regulation of ion channels by integrins. Cell Biochem Biophys **36,** 41, 2002.
101. An, P., and Grabowski, P.J. Exon silencing by UAGG motifs in response to neuronal excitation. PLoS Biol **5,** e36, 2007.
102. Lee, J.A., Xing, Y., Nguyen, D., Xie, J., Lee, C.J., and Black, D.L. Depolarization and CaM kinase IV modulate NMDA receptor splicing through two essential RNA elements. PLoS Biol **5,** e40, 2007.
103. Boutillier, A.L. Depolarization regulates cyclin D1 degradation and neuronal apoptosis: a hypothesis about the role of the ubiquitin/proteasome signalling pathway. Eur J Neurosci **11,** 441, 1999.
104. Rajnicek, A.M., Foubister, L.E., and McCaig, C.D. Temporally and spatially coordinated roles for Rho, Rac, Cdc42 and their effectors in growth cone guidance by a physiological electric field. J Cell Sci **119,** 1723, 2006.
105. Liu, Q.H., Zheng, Y.M., Korde, A.S., Yadav, V.R., Rathore, R., Wess, J., and Wang, Y.X. Membrane depolarization causes a direct activation of G protein-coupled receptors

leading to local Ca2+ release in smooth muscle. Proc Natl Acad Sci U S A **106,** 11418, 2009.
106. Mahaut-Smith, M.P., Martinez-Pinna, J., and Gurung, I.S. A role for membrane potential in regulating GPCRs? Trends Pharmacol Sci **29,** 421, 2008.
107. De, A., Krueger, J.M., and Simasko, S.M. Tumor necrosis factor alpha increases cytosolic calcium responses to AMPA and KCl in primary cultures of rat hippocampal neurons. Brain Res **981,** 133, 2003.
108. Juretic, N., Garcia-Huidobro, P., Iturrieta, J.A., Jaimovich, E., and Riveros, N. Depolarization-induced slow Ca2+ transients stimulate transcription of IL-6 gene in skeletal muscle cells. Am J Physiol Cell Physiol **290,** C1428, 2006.
109. Koller, H., Thiem, K., and Siebler, M. Tumour necrosis factor-alpha increases intracellular Ca2+ and induces a depolarization in cultured astroglial cells. Brain **119,** 2021, 1996.
110. Panáková, D., Werdich, A.A., and MacRae, C.A. Wnt11 patterns a myocardial electrical gradient through regulation of the L-type Ca2+ channel. Nature **466,** 874, 2010.
111. Gregory, C.A., Gunn, W.G., Reyes, E., Smolarz, A.J., Munoz, J., Spees, J.L., and Prockop, D.J. How Wnt signaling affects bone repair by mesenchymal stem cells from the bone marrow. Ann N Y Acad Sci **1049,** 97, 2005.
112. Hartmann, C. A Wnt canon orchestrating osteoblastogenesis. Trends Cell Biol **16,** 151, 2006.

Address correspondence to:
David L. Kaplan, PhD
Department of Biomedical Engineering
Tufts University
4 Colby Street
Medford, MA 02155

E-mail: david.kaplan@tufts.edu

Received: July 12, 2012
Accepted: April 23, 2013
Online Publication Date: June 4, 2013